Received: 10 December 2021 | Revised: 26 January 2022 | Accepted: 31 January 2022

DOI: 10.1002/glia.24158

GLIA

WILEY

RESEARCH ARTICLE

Early targeting of endoneurial macrophages alleviates the neuropathy and affects abnormal Schwann cell differentiation in a mouse model of Charcot-Marie-Tooth 1A

Dennis Klein[1] | Janos Groh[1] | Xidi Yuan[1] | Kristina Berve[1] | Ruth Stassart[2] | Robert Fledrich[3] | Rudolf Martini[1]

[1]Department of Neurology, Developmental Neurobiology, University Hospital Würzburg, Würzburg, Germany

[2]Paul-Flechsig-Institute of Neuropathology, University Clinic Leipzig, Leipzig, Germany

[3]Institute of Anatomy, University of Leipzig, Leipzig, Germany

Correspondence
Dennis Klein, Department of Neurology, Developmental Neurobiology, University Hospital Würzburg, Würzburg, Germany.
Email: klein_d2@ukw.de

Present address
Kristina Berve, Theodor-Kocher-Institute, University of Bern, Bern, Switzerland

Funding information
Federal Ministry of Education and Research; Elitenetzwerk Bayern; Plexxikon

Abstract

We have previously shown that targeting endoneurial macrophages with the orally applied CSF-1 receptor specific kinase (c-FMS) inhibitor PLX5622 from the age of 3 months onwards led to a substantial alleviation of the neuropathy in mouse models of Charcot-Marie-Tooth (CMT) 1X and 1B disease, which are genetically-mediated nerve disorders not treatable in humans. The same approach failed in a model of CMT1A (PMP22-overexpressing mice, line C61), representing the most frequent form of CMT. This was unexpected since previous studies identified macrophages contributing to disease severity in the same CMT1A model. Here we re-approached the possibility of alleviating the neuropathy in a model of CMT1A by targeting macrophages at earlier time points. As a proof-of-principle experiment, we genetically inactivated colony-stimulating factor-1 (CSF-1) in CMT1A mice, which resulted in lower endoneurial macrophage numbers and alleviated the neuropathy. Based on these observations, we pharmacologically ablated macrophages in newborn CMT1A mice by feeding their lactating mothers with chow containing PLX5622, followed by treatment of the respective progenies after weaning until the age of 6 months. We found that peripheral neuropathy was substantially alleviated after early postnatal treatment, leading to preserved motor function in CMT1A mice. Moreover, macrophage depletion affected the altered Schwann cell differentiation phenotype. These findings underscore the targetable role of macrophage-mediated inflammation in peripheral nerves of inherited neuropathies, but also emphasize the need for an early treatment start confined to a narrow therapeutic time window in CMT1A models and potentially in respective patients.

KEYWORDS
colony stimulating factor 1, inherited peripheral neuropathy, macrophage, neuroinflammation, Schwann cell differentiation

1 | INTRODUCTION

In the peripheral nervous system (PNS) macrophages are important players during nerve repair after injury, for example, by phagocytosing myelin debris hence facilitating axonal regrowth (Amann & Prinz, 2020; Brosius Lutz et al., 2017; Cattin et al., 2015; Kolter et al., 2019; Kolter et al., 2020; Martini et al., 2013; Vargas et al., 2010; Ydens et al., 2012; Ydens et al., 2020). Furthermore, these cells were shown to promote Schwann cell maturation and remyelination in regenerated peripheral nerves after lesion (Stratton et al., 2018). However, macrophages can also adopt pathogenic functions under distinct conditions, particularly when activated in apparently non-lesioned nerves. This is the case in Guillain-Barré-syndrome (Goodfellow & Willison, 2018; Ho et al., 1998; Martini & Willison, 2016), in aging peripheral nerves (Yuan et al., 2018), in the course of amyotrophic lateral sclerosis (Trias et al., 2020), during neuropathic pain (Bethea & Fischer, 2021; Shepherd et al., 2018; Sommer et al., 2018) and in the course of genetically-mediated demyelination as it occurs in distinct types of Charcot-Marie-Tooth (CMT) disease (Groh, Klein, Kroner et al., 2015; Klein & Martini, 2016; Martini et al., 2013; Martini & Willison, 2016). In this context, we identified the cytokine CSF-1 as a key molecule for activation of nerve macrophages, initially by crossbreeding CMT1B (Carenini et al., 2001) and CMT1X models (Groh et al., 2012) with functional CSF-1 null mutants (osteopetrotic, op, mice) (Wiktor-Jedrzejczak et al., 1990; Yoshida et al., 1990), and later, by pharmacological targeting the cognate CSF-1 receptor specific kinase (c-FMS) using the specific inhibitor (CSF-1Ri) PLX5622 from 3 months of age onwards (Klein et al., 2015). Both approaches led to a substantial improvement of disease course in two distinct CMT1 models underscoring the pathogenic role of macrophages. Interestingly, macrophage targeting by PLX5622 failed to mitigate neuropathological changes in a model of CMT1A (PMP22tg, C61 mice, Huxley et al., 1998) when treatment started at 3 months of age, although macrophage numbers were substantially reduced upon treatment (Klein et al., 2015). This finding was unexpected as attenuation of macrophage recruitment by CCL2 inactivation demonstrated that macrophages contribute to the pathogenesis in the CMT1A model (Kohl et al., 2010). Here, we re-approached the possibility to treat CMT1A mice by targeting macrophages using PLX5622. Hypothesizing an early start of treatment as being critical for success, we changed the onset of pharmacological macrophage depletion in PMP22tg mice from 3 months of age to newborn mice. We found that peripheral neuropathy in CMT1A mice was indeed substantially alleviated after early start of treatment. In line with these observations, histopathological changes were attenuated in PMP22tg/CSF-1op double mutants, representing a compromised macrophage function in the CMT1A models from the onset. These studies do not only confirm the previously shown pathogenetic impact of macrophages in PMP22tg mice but also identify an early time window for macrophage-directed treatment in models of CMT1A.

2 | MATERIAL AND METHODS

2.1 | Mice

Hemizygous PMP22tg mice of the C61 strain (Huxley et al., 1998) and wild-type littermates of both sexes were investigated at 21 days, 3 and 6 months of age. Additionally, PMP22tg mice were crossbred with CSF-1-deficient osteopetrotic (op) mice (Yoshida et al., 1990) and analyzed at 4 months of age due to reduced vitality of the double mutants (PMP22tg/CSF-1op). This is caused by the spontaneous inactivation of the murine *Csf-1* gene, encoding one of the two ligands of the CSF-1R. The consequent functional impairment of myeloid cells and osteoclasts leads to a general severe phenotype, including osteopetrosis (hence the name) and other life-shortening features (Yoshida et al., 1990). Consequently, and in the context of PMP22 overexpression, double mutants (PMP22tg/CSF-1op) display at least the same detrimental features, including reduced vitality and longevity. Male Cx32def mice (Anzini et al., 1997; Nelles et al., 1996) were analyzed at 4 months of age. All mice were on a C57Bl/6J background, and genotyping was performed by conventional PCR using isolated DNA from ear biopsies according to previously published protocols (Carenini et al., 2001; Kobsar et al., 2003; Kohl et al., 2010). Animals were kept in individually ventilated cages (IVC) under barrier conditions at the Center of Experimental Molecular Medicine, University of Würzburg with a 14 h/10 h day/night rhythm (<300 lux during day). Colonies were maintained at 20–24°C and 40%–60% humidity, with free access to food and water. All animal experiments were approved by the local authority of the Government of Lower Franconia, Germany.

2.2 | PLX5622 (CSF-1R inhibitor) treatment and determination of PLX5622 levels in plasma

Rodent chow containing 300 mg/kg CSF-1 receptor specific kinase (c-FMS) inhibitor (termed hereafter PLX5622) was provided by Plexxikon Inc. In order to perform an early postnatal treatment of mice, their lactating mothers were treated with PLX5622 from the day of birth of the progeny. After weaning, treatment continued in mice by feeding the respective chow containing PLX5622 ad libitum for up to 4 (Cx32def) or 6 months of age (PMP22tg). During the experiments, animals were monitored individually. No mice had to be excluded based on problems in health and behavior (http://www.stabsstelleau.zv.uniwuerzburg.de/?id=49517).

To determine PLX5622 concentrations in 21 days old pups by mass spectrometry, plasma was collected after centrifugation of heparinized blood which was obtained by cardiac puncture from untreated control and treated animals (directly after asphyxiation with CO_2, see below). Bioanalysis of PLX5622 by liquid chromatography–tandem mass spectrometry (LC/MS/MS) was conducted by Plexxikon Inc. as previously described (Klein et al., 2015).

2.3 | Nerve dissection and tissue processing

Animals were sacrificed by asphyxiation with CO_2 (according to guidelines by the State Office of Health and Social Affairs, Berlin) as previously described (Klein et al., 2021). Blood was removed by transcardial perfusion with phosphate buffered saline (PBS) containing heparin. For immunohistochemistry of fresh frozen tissue, femoral nerves (comprising the quadriceps and saphenous branch) and flexor digitorum brevis muscles were freshly dissected, embedded in Tissue-Tek® O.C.T. compound (Sakura), and frozen in liquid nitrogen-cooled methylbutane. Fresh frozen tissues were then cut into 10-μm-thick cross sections on a cryostat (Leica) and stored at −20°C. For isolation of total RNA, tissue was snap frozen in liquid nitrogen and stored at −80°C until use.

For electron microscopy, mice were transcardially perfused with 4% PFA and 2% glutaraldehyde in 0.1 M cacodylate buffer for 15 min. Dissected femoral nerves and lumbar ventral roots were subsequently post-fixed in the same solution overnight at 4°C. Osmification was performed with 2% osmium tetroxide in 0.1 M cacodylate buffer for 2 h, followed by dehydration in ascending acetone concentrations. Nerve tissue was embedded in Spurr's medium. Ultrathin sections (70 nm) were cut and mounted to copper grids and counterstained with lead citrate.

2.4 | Immunohistochemistry

Quantification of total numbers and the assessment of activation of endoneurial macrophages as well as of abnormal Schwann cell differentiation was performed on cross sections according to previously published protocols (Klein et al., 2014; Klein et al., 2015). To quantify absolute numbers of macrophages, samples were blocked with 5% bovine serum albumin (BSA) in PBS and then incubated at 4°C with an antibody against the pan-macrophage marker, F4/80 (rat, 1:300, MCAP497, Serotec) in 1% BSA in PBS overnight. After washing with PBS, samples were incubated with Cy3-conjugated goat anti-rat IgG (1:300, 112–165-167, Dianova) secondary antibodies for 1 h at room temperature. Using additional macrophage activation markers, immunohistochemical stainings against CD86 or CD206 were performed. Samples were fixed in acetone (10 min, −20°C), blocked with 5% BSA in PBS, and incubated overnight at 4°C with anti-CD86 (rat, 1:100, 553,688, BD Pharmingen) or anti-CD206 (rat, 1:2000, MCA 2235, Serotec) primary antibodies in PBS containing 1% BSA. Primary antibodies were detected by the corresponding Cy3-conjugated secondary antibody (1:300, 112–165-167, Dianova). In case of the CD206 antibody, 0.3% TritonX-100 was added to the blocking and antibody solutions. Nuclei were stained with DAPI (Sigma-Aldrich). On 7–10 consecutive sections per animal, the mean numbers of F4/80-, CD86-, or CD206-positive cells per section were determined. Percentages of CD86- or CD206-positive profiles were calculated based on the total macrophage number shown by quantification of F4/80-positive profiles.

To determine abnormal Schwann cell differentiation, an immunohistochemical staining with a protocol similar as above (see F4/80) was performed using an antibody against NCAM (goat, 1:300, AF2408, R&D Systems) and a corresponding secondary antibody (1:300, 705–165-147, Dianova). On 7–10 consecutive sections per animal, the mean number of all NCAM+ profiles, NCAM+ myelinating Schwann cells and NCAM+ "non-myelin" profiles, most likely representing supernumerary Schwann cells (Guenard et al., 1996), were quantified. Non-myelinating Schwann cells of Remak fibers, which are also strongly positive for NCAM, were excluded in the quantification (Klein et al., 2014). To further demonstrate the presence of NCAM on myelinating and supernumerary Schwann cells, a double immunohistochemical staining against NCAM (see above) and MPZ/P0 (chicken, 1:500, AP31820PU-N, Origene) with corresponding secondary antibodies (donkey, 1:300, Dianova) was performed on nerve cross sections. In this case, 0.1% TritonX-100 was also added to the blocking and antibody solutions to facilitate antibody penetration into myelin.

Visualization of type 1 and type 2 muscle fibers in flexor digitorum brevis muscles was performed by actomyosin ATPase histochemistry at pH 4.3 on muscle cryosections as described previously (Frei et al., 1999). For the determination of muscle fiber size, randomly selected regions in the muscle were chosen, and the perimeter of every individual fiber was analyzed (muscle spindles were excluded). Fibers with a perimeter <50 μm were considered as "atrophic".

Digital fluorescence microscopic images were acquired using an Axiophot 2 microscope (Zeiss) equipped with a CCD camera (Visitron Systems) or an Axio Imager M2 microscope (Zeiss) with ApoTome.2 structured illumination equipment, attached Axiocam cameras and corresponding software (ZEN v.2.3 blue edition). Images were minimally processed (rotation, cropping, addition of symbols) with Photoshop 2021 (Adobe) or ImageJ (National Institutes of Health).

2.5 | Morphological analysis by electron microscopy

Electron microscopic images were taken using a ProScan Slow Scan CCD camera mounted to a Leo 906E electron microscope (Zeiss). Multiple images were aligned with the software iTEM (Olympus Soft Imaging Solutions) to analyze whole nerve cross sections. Pathological alterations were determined in relation to the total number of axons in corresponding cross sections of the femoral quadriceps nerves or lumbar ventral roots. De- and thinly myelinated axons, supernumerary Schwann cells (onion bulbs) and degenerating/degenerated axons were quantified. Degenerating/degenerated axons were defined as axons that have lost their normal integrity of cytoskeletal elements or detaching from the inner loop and leaving empty myelin sheaths, as well as denervated Schwann cell profiles reminiscent of Büngner bands. Moreover, the axon caliber and respective g-ratio were analyzed in randomly selected high magnification images. Approximately 100 myelinated axons per mouse were examined. Additionally, foamy macrophages were counted, and their numbers were given as relative values per 100 axons within the nerve.

2.6 | RNA extraction and semi-quantitative real-time PCR (qPCR)

Total RNA was extracted from femoral quadriceps nerves at indicated time-points semi-automated using a Maxwell® RSC (Promega) and the Maxwell® RSC simplyRNA Tissue Kit (Promega) according to the manufacturer's instructions. In short, fresh frozen nerve samples were mechanically homogenized in homogenization solution using the prechilled Bead Ruptor 24 (Omni). Tissue homogenate was then mixed with 200 µl lysis buffer and loaded onto the prepared cartridge. The cartridge was then placed into the Maxwell® RSC (Promega) machine and RNA further isolated and purified automatically according to the manufacturers protocol. Integrity, purity, and quantity of isolated RNA were assessed using the Agilent 5200 Fragment Analyzer System (Agilent Technologies). For quantitative real-time PCR (qPCR), total RNA was reversely transcribed into cDNA using the Superscript IV Reverse Transcriptase (Thermo Fisher) and poly-Thymine together with random nonamer primer. qPCRs were performed in quadruplets using the GoTaq qPCR Master Mix (Promega) in a qTower3 light cycler (Analytik Jena). CT values were calculated by the qPCRsoft (Analytik Jena) and transformed into fold-change expression. Fold-change values of the control group were normalized to 1 and the fold-change values of experimental groups were depicted relative to the control group. *Rictor*, *Ankrd27*, and *Ppia* were used as housekeeping genes. Primer sequences are depicted in Table S1 and the following amplification protocol was used: 2 min warm up at 50°C, 10 min GoTaq activation at 95°C, 60 s annealing/elongation at 60°C, 15 s denaturation at 95°C, 40 cycles of annealing/elongation/denaturation with a ramping rate of 1°C per 0.15 s.

2.7 | Nerve conduction studies

Mice were anesthetized by an intraperitoneal injection with a mixture of Ketavet (Pfizer) and Xylavet (CP-Pharma) (100 mg Ketavet and 6.7 mg Xylavet per kilogram bodyweight) and were placed under a heating lamp to avoid hypothermia. Body temperature of mice was monitored before and after measurements (34–36°C). Electrophysiological properties of the left sciatic nerve were measured as described previously (Klein et al., 2021; Zielasek et al., 1996). Shortly, after supramaximal stimulation of the tibial nerve with monopolar needle electrodes at the ankle (distal) and the sciatic nerve at the sciatic notch (proximal), compound muscle action potentials (CMAPs, not shown in this study) were recorded from hind paw muscles using steel needle electrodes. Distal and proximal latencies as well as the distance between stimulation sites were measured. The corresponding nerve conduction velocity (NCV) was calculated by the distance between stimulation sites divided by the difference between proximal and distal latencies. All neurographic recordings were performed with a digital Neurosoft-Evidence 3102 electromyograph (Schreiber & Tholen Medizintechnik).

2.8 | Grip test

Grip strength of the hindlimbs was measured using an automated Grip Strength Meter (Columbus Instruments) as described previously (Klein et al., 2021). With forelimbs supported by a metal grid, mice were trained to hold a grip bar properly with hind paws. The maximum force (in newton) was measured when the mouse was pulled off the grip bar with constant strength. Ten measurements per day were performed on three consecutive days and the mean of the measurements was calculated.

2.9 | Statistical analysis

All experiments were performed with the investigators not aware of the genotype and the experimental status of the analyzed mice. Animals were randomly placed into experimental or control groups according to genotyping results using a random generator (http://www.randomizer.org). Biometrical sample size estimation was performed with G*Power (Faul et al., 2007). Calculation of appropriate sample size groups was performed using an a priori power analysis by comparing the mean of 3–4 groups with a defined adequate power of 0.8 (1 – beta error) and an α error of 0.05. To determine the prespecified effect size *d*, previously published data were considered as comparable reference values (Groh et al., 2010; Klein et al., 2015; Yuan et al., 2018). Statistical analyses were performed using Prism 8 (GraphPad). Data sets were tested for normal distribution and variance homology. If more than two groups were compared, differences among normally distributed data were tested by one-way ANOVA, followed by Tukey's post hoc test. Student's t-test was used to compare two groups with normally distributed data and similar variance. Otherwise, Welch's t-test was used to determine the significance of differences. In the case of not normally distributed datasets, the nonparametric Kruskal-Wallis test with Dunn's post hoc test was applied. Significance levels (#, *$p < .05$; ##, **$p < .01$; ###; ***$p < .001$) are indicated together with the applied statistical tests within the figure legends, with # showing significant differences to (untreated) WT mice and * showing significant differences between corresponding mutant mice. For analyzing the distribution of g-ratio against axon diameter, a regression analysis was performed to compare whether slopes differ significantly. Measurements and quantifications are shown as individual values (*n*-numbers are represented in the graphs as circles) and mean ± *SD*, unless stated otherwise. For EM analysis, only PMP22tg mice (control and CSF-1op or untreated and PLX5622 treated, respectively) were statistically compared without WT groups, as indicated in the respective figure legends. Graphs were generated with Prism 8.

3 | RESULTS

3.1 | Genetic inactivation of CSF-1 mitigates the neuropathy in PMP22tg mice

To determine if the CSF-1/CSF-1R axis mediates the increase of endoneurial macrophage numbers and demyelination, as it was previously

shown for mouse models of CMT1B (Carenini et al., 2001) and CMT1X (Groh et al., 2012), PMP22tg (C61) mice were crossbred with CSF-1 deficient mice (Yoshida et al., 1990). As reported earlier (Kobsar et al., 2005; Kohl et al., 2010), PMP22tg mice showed elevated numbers of F4/80+ endoneurial macrophages by immunohistochemistry, as well as myelin-phagocytosing macrophages identified by electron microscopy, compared with wild-type (WT) mice (Figure 1). By contrast, PMP22tg mice deficient for CSF-1 showed lower numbers of endoneurial macrophages at 4 months, which was the oldest age investigated due to reduced longevity of the double mutants (see Material and Methods, Section 2). These results demonstrate that macrophage activation in peripheral nerves of PMP22tg mice is at least partially mediated by CSF-1 (Figure 1). Importantly, CSF-1 deficiency also reduced the number of demyelinated axons in quadriceps nerves (Figure 2a,b) and showed a trend towards reduced numbers of thinly myelinated axons and supernumerary Schwann cells in quadriceps nerves of PMP22tg mice (Figure 2c,d). Moreover, demyelinating features and numbers of foamy macrophage were significantly lower in lumbar ventral roots of PMP22tg/CSF-1op compared with PMP22tg mice (Figure S1). In contrast, hypermyelinated axons, a specific histopathological peculiarity of PMP22tg mice (Kobsar et al., 2005; Kohl et al., 2010), were not affected by CSF-1 deficiency (data not shown). These proof-of-principle experiments with a limited number of mice were sufficient to demonstrate a partial impact of the CSF-1/CSF-1R axis in the demyelinating phenotype of PMP22tg mice and corroborate and extend our previous findings on the pathogenic role of the CSF-1/CSF-1R axis in two other CMT1 models (Carenini et al., 2001; Groh et al., 2012).

3.2 | Early postnatal PLX5622 treatment reduces macrophage activation and mitigates the neuropathy in PMP22tg mice, resulting in preserved motor function

What might explain the discrepancy regarding disease amelioration between genetic inactivation of CSF-1 and the previously performed pharmacological blockade of the CSF-1R by PLX5622? We here hypothesize that pharmacological intervention from 3 months of age onwards might have been too late for an effective treatment of

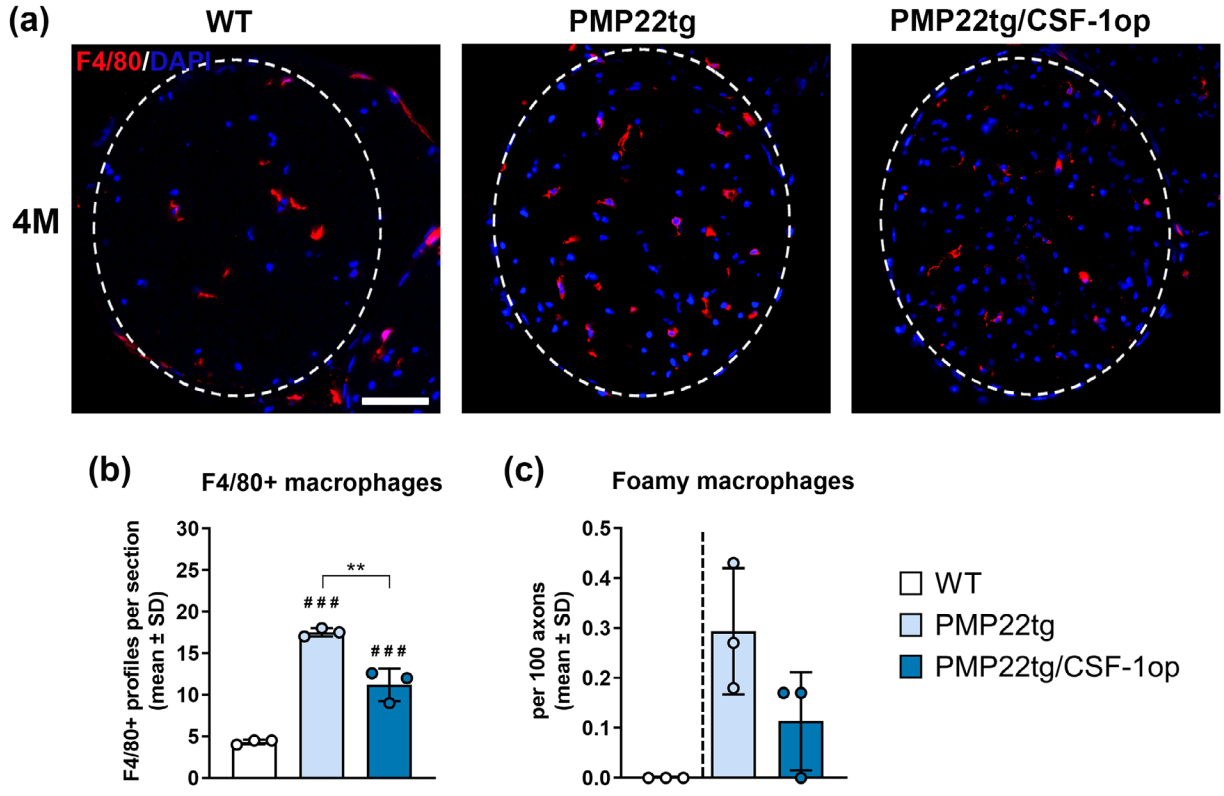

FIGURE 1 CSF-1 contributes to the increase of macrophage numbers in peripheral nerves of PMP22tg mice. (a) Immunohistochemical staining against the macrophage pan-marker F4/80 on cross-sections of femoral nerves from 4-month-old WT (left), PMP22tg (middle) and PMP22tg/CSF-1op mice (right). Dashed circles represent the area of femoral quadriceps nerves. Nuclei are labeled with DAPI. Scale bar, 50 μm. (b) Corresponding quantification of F4/80-positive profiles in femoral quadriceps nerves. There is a significant increase of macrophage numbers in both PMP22tg mutant groups compared with WT mice (#). Note that CSF-1 deficiency (CSF-1op) results in a significantly lower increase of macrophage numbers compared with PMP22tg mice (*). One-way ANOVA and Tukey's post hoc tests; $^{**}p < .01$; ###, $^{***}p < .001$. (c) Electron microscopy-based quantification of foamy macrophages reveals a non-significant trend towards lower numbers of phagocytosing macrophages in femoral quadriceps nerves from 4-month-old PMP22tg/CSF-1op compared with PMP22tg mice. Foamy macrophages are not detectable in WT nerves. Only PMP22 mutant mice are compared statistically, as indicated by the black dashed line. Two-tailed Student's *t*-test

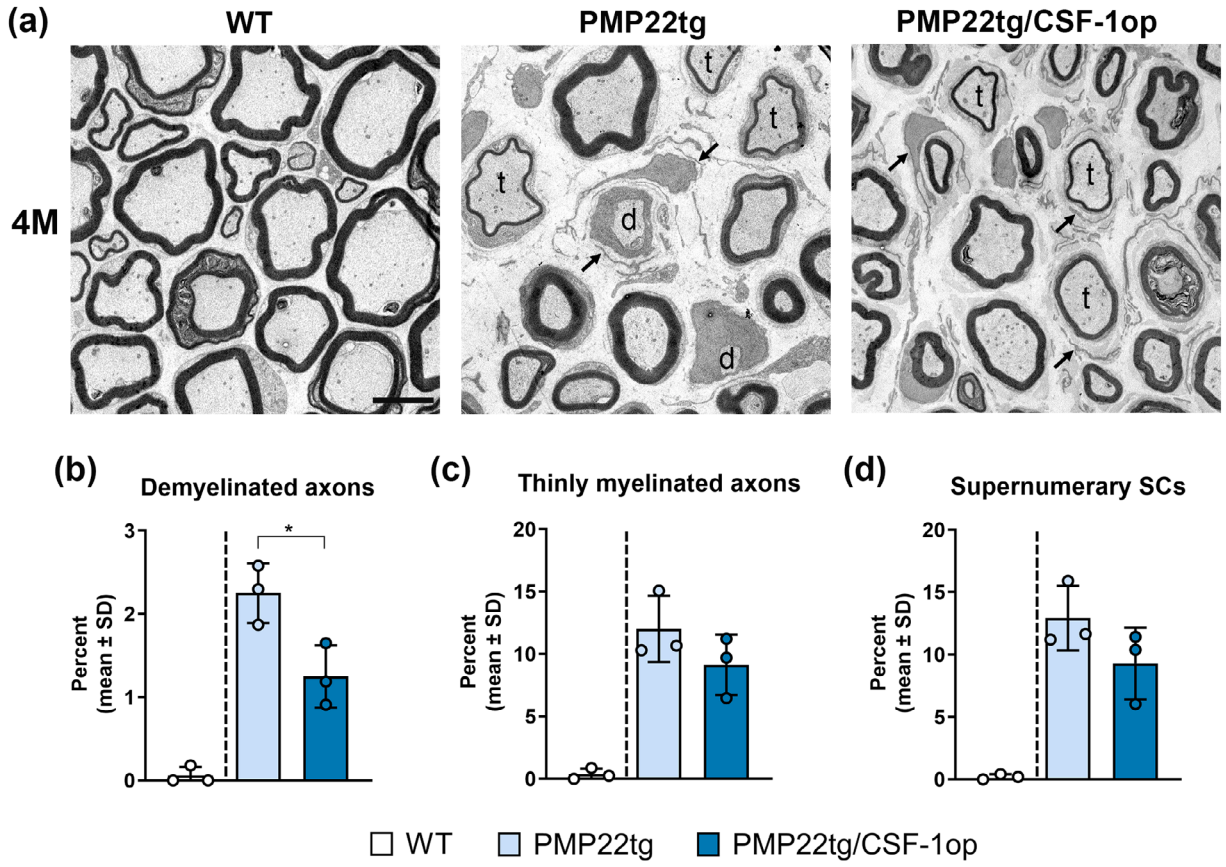

FIGURE 2 CSF-1 deficiency alleviates the demyelinating phenotype in PMP22tg mice. (a) Representative electron micrographs of femoral quadriceps nerves from 4-month-old WT (left), PMP22tg (middle) and PMP22tg/CSF-1op mice (right). Typical histopathological alterations such as demyelinated (d) and thinly myelinated (t) axons as well as supernumerary Schwann cells (onion bulbs; arrow) are detectable in nerves of PMP22 mutant mice. Scale bar, 5 μm. (b–d) Quantification of demyelinated fibers reveals a significantly lower percentage in PMP22tg/CSF-1op compared with PMP22tg mice (b), whereas thinly myelinated fibers (c) and supernumerary Schwann cells (SCs, onion bulbs) (d) only show a trend towards lower percentages. These pathological alterations are barely seen in WT nerves. Only PMP22 mutant mice are compared statistically, as indicated by the black dashed line. Two-tailed Student's *t*-test; $^*p < .05$

PMP22tg mice. Consequently, we started early postnatal treatment of PMP22tg mice (Figure 3a) by feeding already lactating mothers with the CSF-1R inhibitor. This led to serum levels of PLX5622 in 21-day-old pups comparable to those seen in weaned mice that were directly fed with the inhibitor (Figure S2a; 11.45 ± 2.43 μM, Klein et al., 2015). Importantly, early PLX5622 treatment depleted 60%–70% of nerve macrophages that were already accumulating in untreated 21-day-old PMP22tg compared with WT mice (Figure S2b). Quantification of macrophages expressing the activation markers mannose receptor (CD206) or CD86 (Klein et al., 2021) revealed an equal reduction by early PLX5622 treatment, suggesting that the activation of macrophages remained unaffected by the treatment (Figure S2c–f).

After weaning (at approximately 4 weeks of age), PLX5622 treatment was continued by feeding with the respective chow until up to 6 months of age. At the end of treatment, numbers of F4/80+ macrophages in femoral quadriceps nerves were reduced by approximately 70% in WT and PMP22tg mice (Figure 3b, c), comparable to our previous observations in mice treated from postnatal month three onwards (Klein et al., 2015). Additionally, significantly fewer myelin-phagocytosing macrophages were detectable in femoral quadriceps nerves of PMP22tg mice after early-onset PLX5622 treatment (Figure 3d). The impact on macrophages was not confined to the quadriceps nerves, as the increase of macrophage numbers in the pure sensory saphenous nerves in PMP22tg compared to WT mice was also blocked after PLX5622 treatment (Figure S2g,h). However, as demyelinating features are much milder in this nerve (Kobsar et al., 2005) we decided to focus in the following on the quadriceps nerve that shows more robust pathological features.

In line with our observations in PMP22tg/CSF-1op mice, early PLX5622 treatment resulted in a robust amelioration of the pathological changes in quadriceps nerves of PMP22tg mutants at 6 months of age, as both de- and thinly myelinated axons were significantly reduced in numbers compared to untreated controls (Figure 4a–c). In contrast, supernumerary Schwann cells only showed a mild tendency towards a lower frequency after PLX5622 treatment (Figure 4d), resulting in their increased association with normally myelinated axons in treated PMP22tg mice (Figure 4e, f). Hypermyelinated axonal

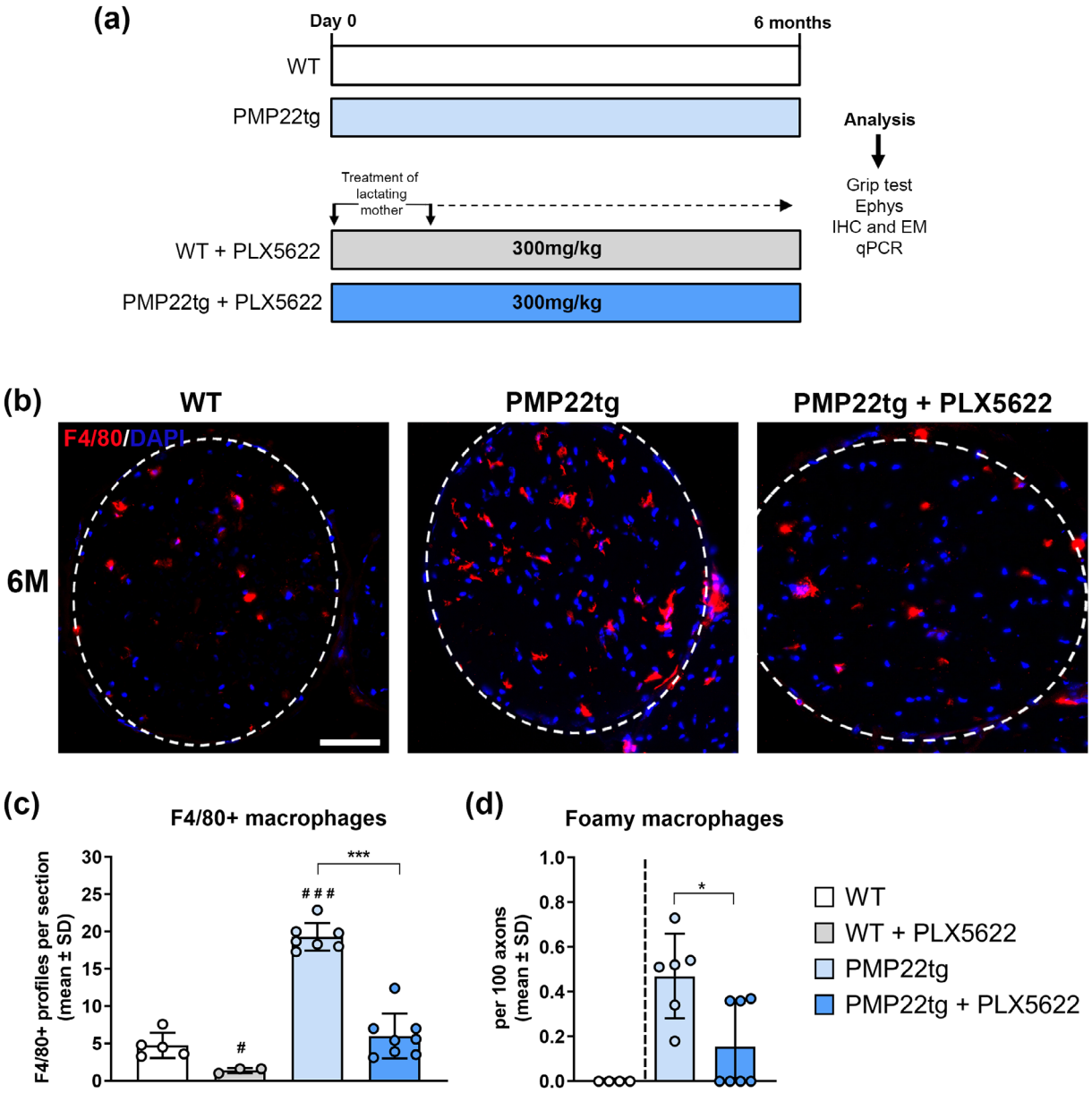

FIGURE 3 Early postnatal macrophage targeting reduces macrophage numbers in peripheral nerves of PMP22tg mice. (a) Schematic representation of the treatment regimen using PLX5622 (CSF-1R inhibitor, 300 mg/kg). For early postnatal treatment of mice, their lactating mothers were treated with PLX5622 from the day of birth of the progeny. After weaning, treatment continued in WT and PMP22tg mice. Treated animals were analyzed in comparison with untreated control animals at 6 months of age. (b) Immunohistochemical staining against the macrophage pan-marker F4/80 on cross-sections of femoral nerves from 6-month-old WT (left), PMP22tg (middle) and PLX5622 treated PMP22tg mice (right). Dashed circles represent the area of femoral quadriceps nerves. Nuclei are labeled with DAPI. Scale bar, 50 μm. (c) Corresponding quantification of F4/80-positive profiles in femoral quadriceps nerves shows a significant increase of macrophage numbers in PMP22tg mice compared with WT mice (#). Note that early postnatal PLX5622 treatment significantly reduces the number of macrophages in WT (#) and PMP22tg mice (*). One-way ANOVA and Tukey's post hoc tests; #$p < .05$; ###, ***$p < .001$. (d) Quantification of foamy macrophages reveals significantly reduced numbers of phagocytosing macrophages in femoral quadriceps nerves from 6-month-old PLX5622 treated PMP22tg compared with PMP22tg mice. Foamy macrophages are not detectable in WT nerves. Only PMP22 mutant mice are compared statistically, as indicated by the black dashed line. Two-tailed Student's *t*-test; *$p < .05$

profiles were not affected by early PLX5622 treatment (data not shown), comparable to our observations in PMP22tg/CSF-1op mice. To get further insight into myelin thickness, g-ratio analysis (axonal diameter/fiber diameter) was performed in femoral quadriceps nerves. A steeper slope (g-ratio plotted against axon diameter) in PMP22tg compared with WT mice represented the high frequency of hypermyelinated small axons and thinly myelinated middle- and large-caliber axons in the mutants (Figure 4h; Figure S3a).

Interestingly, early PLX5622 treatment led to thicker myelin mostly in large caliber axons (>7 μm), without affecting hypermyelinated small axons (see also above) (Figure 4i; Figure S3a). Of note, features indicative of demyelination were only transiently reduced in ventral roots of PLX5622 treated PMP22tg mice, as demyelination was only ameliorated at 3 but not at 6 months of age (Figure S3b–h).

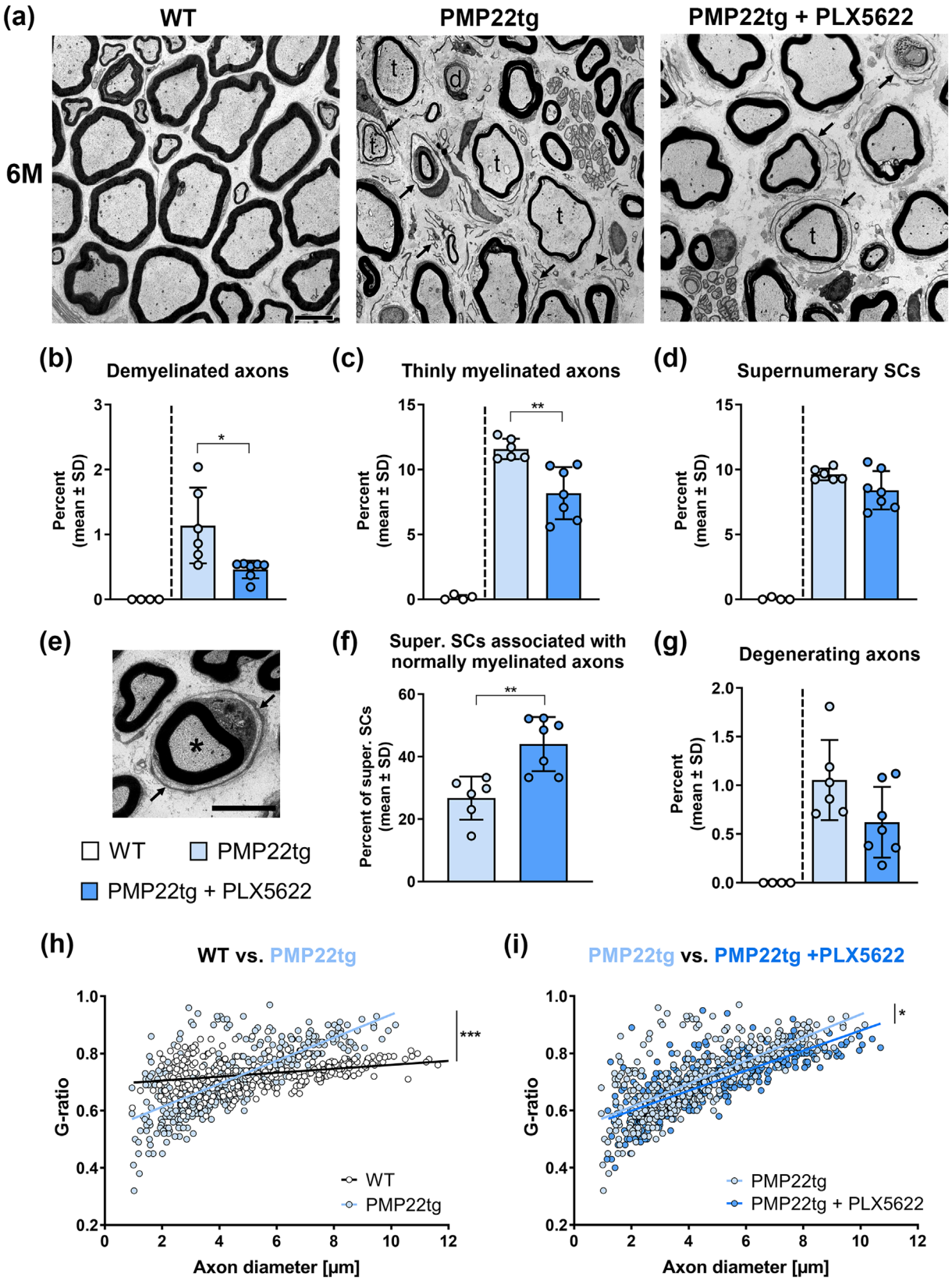

FIGURE 4 Legend on next page.

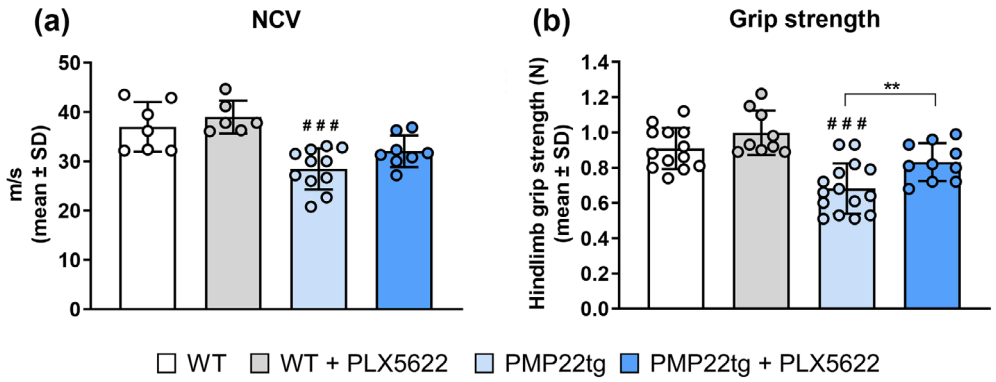

FIGURE 5 Early postnatal macrophage targeting partially prevents functional impairment in PMP22tg mice. (a) Quantification of nerve conduction velocity (NCV) in 6-month-old mice. Early postnatal PLX5622 treatment attenuates the significant NCV reduction observed in untreated PMP22tg mice compared with WT mice (#). PLX5622 treatment has no effect on NCV in WT mice. One-way ANOVA and Tukey's post hoc tests; ### $p < .001$. (b) Analysis of hind limb grip strength demonstrates a significant reduction in untreated PMP22tg compared with WT mice at 6 months of age (#). This is prevented by early postnatal PLX5622 treatment in PMP22tg mice (*). PLX5622 treatment has no effect on grip strength in WT mice. One-way ANOVA and Tukey's post hoc tests; **$p < .01$; ###$p < .001$

Next, we investigated whether the ameliorated neuropathological features contribute to an improved functional outcome. Clinically, early PLX5622 treatment prevented a significant decline of motor nerve conduction velocity (NCV, Figure 5a) and hindlimb grip strength at 6 months of age in PMP22tg mutants (Figure 5b). These observations were going along with a trend towards less abnormally innervated (comprising both denervated and partially denervated) neuromuscular junctions (NMJs) in the flexor digitorum brevis (FDB) muscle (Figure S4a). However, CMAP amplitudes were not affected by early PLX5622 treatment (data not shown). Histochemical labeling of ATPase (at pH = 4.3) on FDB sections revealed a smaller diameter of both type 1 (stained, slow twitch) and type 2 (not stained, fast twitch) muscle fibers in PMP22tg compared to WT mice (Figure S4b–f). Of note, early PLX5622 treatment partially corrected this phenotype (Figure S4b–f), possibly contributing to the preserved muscle function (Figure 5b).

Together, these data suggest that early postnatal macrophage targeting is necessary for mitigating neuropathic changes and functional decline in PMP22tg mice, possibly explaining the inefficacy of our previous PLX5622 treatment approach in this model (Klein et al., 2015).

3.3 | Early postnatal PLX5622 treatment modulates the abnormal differentiation phenotype of PMP22tg Schwann cells

In another established CMT1A model, the PMP22-transgenic rat, Schwann cells display an abnormally differentiated, immature phenotype, which is driven by increased MEK–ERK signaling. This leads to further dedifferentiation of Schwann cells and loss of myelin and

FIGURE 4 Early postnatal macrophage targeting alleviates some demyelinating features in PMP22tg mice. (a) Representative electron micrographs of femoral quadriceps nerves from 6-month-old WT (left), PMP22tg (middle) and PLX5622 treated PMP22tg mice (right). Typical histopathological alterations such as demyelinated (d) and thinly myelinated (t) axons as well as supernumerary Schwann cells (onion bulbs; arrow) and degenerated axons (Büngner bands, arrowhead) are detectable in nerves of PMP22 mutant mice. Scale bar, 5 μm. (b–d) Quantification of demyelinated (b) and thinly myelinated fibers (c) reveals significantly lower percentages in PLX5622 treated PMP22tg compared with untreated PMP22tg mice, whereas supernumerary Schwann cells (SCs, onion bulbs) (d) only show a mild trend towards lower percentages. These pathological alterations are barely seen in WT nerves. Only PMP22 mutant mice are compared statistically, as indicated by the black dashed line. Two-tailed Student's *t*-test; *$p < .05$; **$p < .01$. (e) Representative electron micrograph of a supernumerary Schwann cell (arrow) surrounding a normally myelinated axon (indicated by *) in femoral quadriceps nerves from a 6-month-old PLX5622 treated PMP22tg mouse. Scale bar, 5 μm. (f) Quantification of supernumerary SCs around normally myelinated axons shown as the percentage of supernumerary SCs from (d). Early postnatal PLX5622 treatment results in significantly higher frequency of these profiles compared with untreated PMP22tg mice. Two-tailed Student's *t*-test; **$p < .01$. (g) Quantification of degenerating/degenerated axons shows a non-significant reduction in their percentage in PLX5622 treated PMP22tg compared with untreated PMP22tg mice. These pathological profiles are not seen in WT nerves. Only PMP22 mutant mice are compared statistically, as indicated by the black dashed line. Two-tailed Student's *t*-test. (h,i) Scatter plot graphs displaying g-ratio (y-axis) in relation to axon diameter (x-axis) of individual fibers, represented by single dots and the corresponding linear regression. WT (black) is shown against untreated PMP22tg (light blue, h), and untreated PMP22tg (light blue) against PLX5622 treated PMP22tg (dark blue, i). A significantly steeper slope is detectable in PMP22tg compared with WT mice (h). Note that early postnatal PLX5622 treatment in PMP22tg mice leads to a shift of middle and large caliber axons towards lower g-ratios, thereby changing the slope significantly. Hypermyelinated small caliber axons are not affected by treatment in PMP22tg mice (i). Linear regression with ANCOVA analysis. See also Figure S3a

axons over time (Fledrich et al., 2014). Since macrophage activation occurs downstream of MEK–ERK signaling (Fischer et al., 2008; Groh et al., 2010; Kohl et al., 2010) and also influences the differentiation state of myelin mutant Schwann cells (Groh, Klein, Hollmann, et al., 2015), we here investigated the possibility that macrophages contribute to the abnormal differentiation process of Schwann cells in PMP22tg mice.

A particularly interesting marker of Schwann cell dedifferentiation is neural cell adhesion molecule (NCAM) (Klein et al., 2014). Previous studies in WT mice showed that this adhesion molecule is normally nearly absent from myelin (Martini & Schachner, 1986) and only detectable in Schwann cells associated with Remak fibers. However, in dysmyelinating mutants, such as P0−/− (Giese et al., 1992) and PMP22tg mice (Klein et al., 2014), NCAM is additionally present in

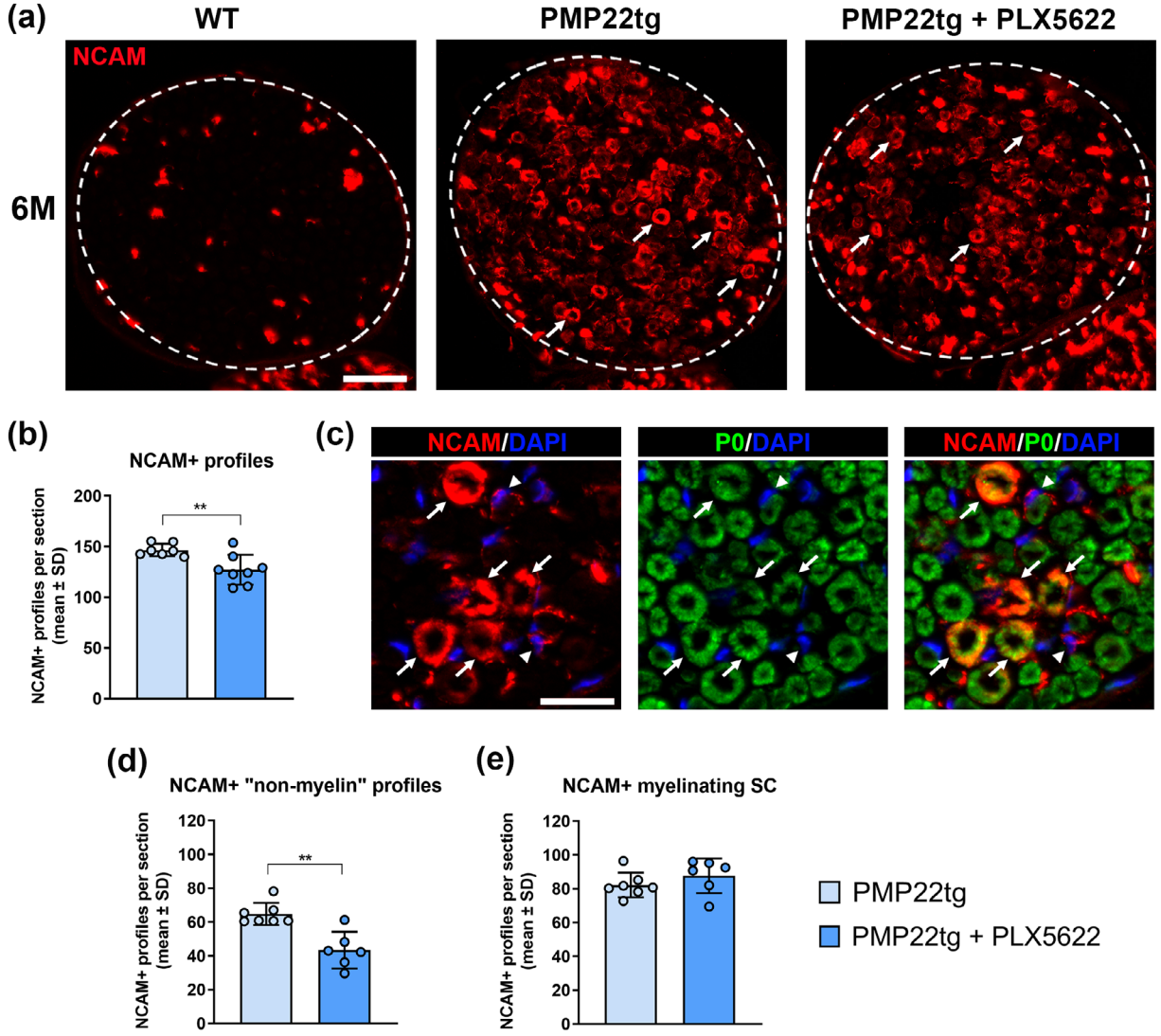

FIGURE 6 Early postnatal macrophage targeting reduces some aspects of Schwann cell differentiation defects in PMP22tg mice. (a) Immunohistochemical staining against NCAM on cross-sections of femoral quadriceps nerves from 6-month-old WT (left), PMP22tg (middle) and PLX5622 treated PMP22tg mice (right). Note the circular profiles representing NCAM-positive myelin profiles (arrow, see also Figure 6c) and the overall abundant increase of NCAM-positive structures representing supernumerary Schwann cells (see also Figure 6c). Remak fibers, the only NCAM-positive structures in WT nerves (left), are strongly labeled in all groups and not considered for further quantification. Dashed circles represent the area of femoral quadriceps nerves. Scale bar, 50 μm. (b) Corresponding quantification of NCAM-positive profiles (excluding Remak bundles) in femoral quadriceps nerves shows a significant alleviation of the Schwann cell differentiation defect in PLX5622 treated compared with untreated PMP22tg mice (*). Two-tailed Student's *t*-test; $^{**}p < .01$. (c) Immunohistochemical staining against NCAM and P0 (MPZ) on cross-sections of femoral quadriceps nerves from 6-month-old PMP22tg mice. NCAM-positive profiles associated with some, but not all, P0-positive myelin/myelinating Schwann cells (SC, arrow) or supernumerary SCs surrounding (NCAM-negative) myelinated axons (arrowhead) are indicated. Note the different intensities in immunoreactivity of NCAM-positive myelin profiles. Scale bar, 20 μm. (d) Quantification of NCAM-positive "non-myelin" profiles, reflecting supernumerary SCs, in femoral quadriceps nerves shows a significant reduction in PLX5622 treated compared with untreated PMP22tg mice (*). Two-tailed Student's *t*-test; $^{**}p < .01$. (e) Quantification of NCAM-positive profiles associated with myelin/myelinating SC in femoral quadriceps nerves reveals no effect of early onset PLX5622 treatment in PMP22tg mice. Two-tailed Student's *t*-test

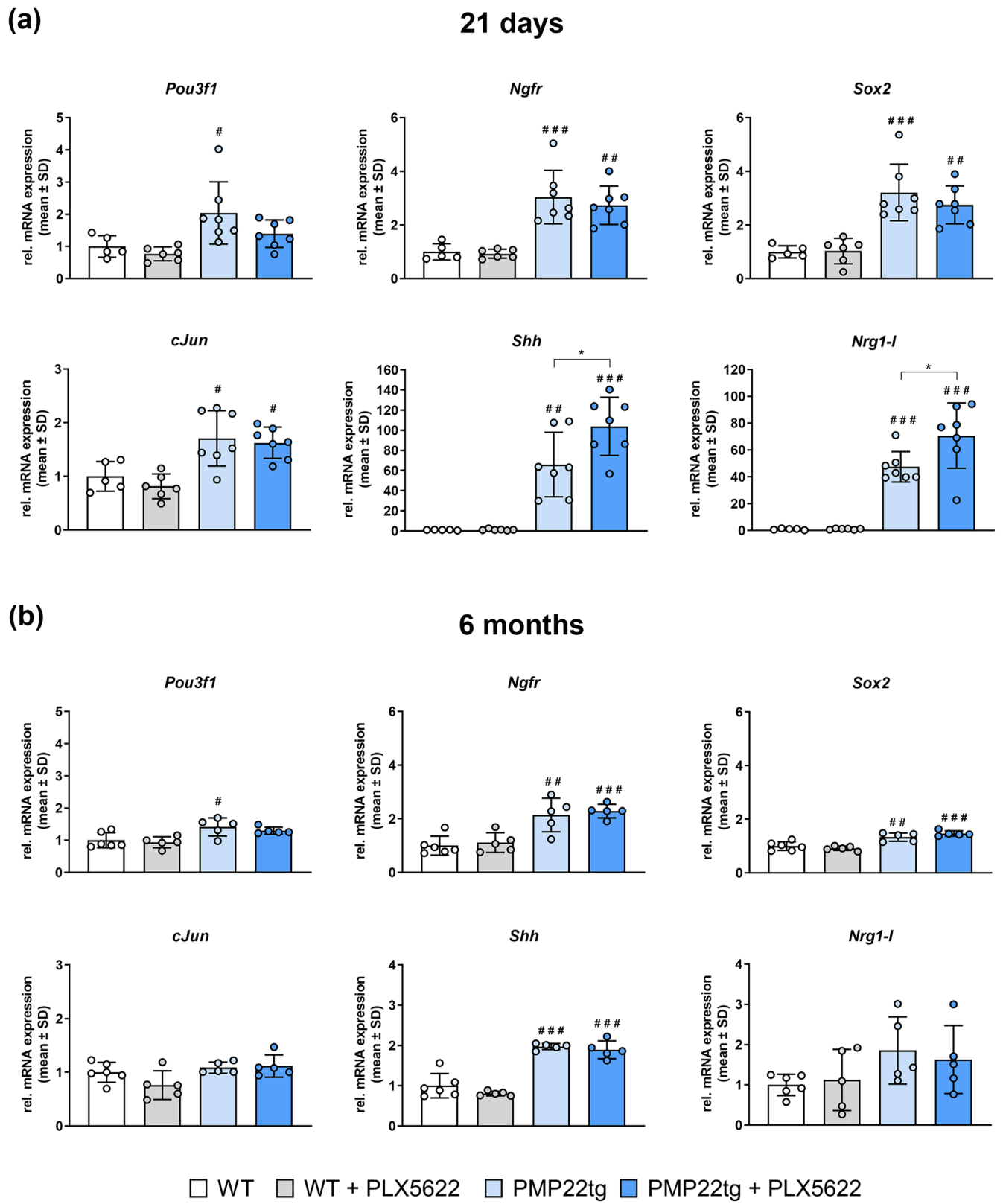

FIGURE 7 Early postnatal macrophage targeting modulates the Schwann cell differentiation defect in PMP22tg mice. (a,b) Relative mRNA expression of *Pou3f1*, *Ngfr*, *Sox2*, *cJun*, *Shh* and *Nrg1-I* in 21-day- (a) and 6-month-old (b) femoral quadriceps nerves. *Pou3f1*, *Sox2* and *Ngfr* are significantly upregulated in untreated PMP22tg compared with WT mice at P21 (a) and 6 M (b). Early PLX5622 treatment has no effect on the expression of these "immaturity genes". The expression of the genuine dedifferentiation markers *Shh* and *Nrg1-I* was highly increased in untreated PMP22tg compared with WT mice at P21, but not at 6 M. Note that early postnatal PLX5622 treatment significantly increases the mRNA expression of *Shh* and *Nrg1-I* compared with untreated PMP22tg mice at P21 (a), but not at 6 months of age (b). PLX5622 treatment has no effect on the expression of any of these marker genes in WT mice at both investigated time points. One-way ANOVA and Tukey's post hoc tests; #, $^{*}p < .05$; ##$p < .01$; ###$p < .001$

myelin profiles. Accordingly, PMP22tg mice showed a high number of NCAM+ profiles (excluding Remak bundles) in femoral quadriceps nerves at 6 months of age, which were significantly reduced upon PLX5622 treatment (Figure 6a, b). Further classifying NCAM+ profiles, we identified supernumerary Schwann cells as NCAM positive structures (Figure 6c), as also previously described (Guenard et al., 1996; Hanemann et al., 1997; Klein et al., 2014). Of note, we observed significantly fewer of these profiles in PLX5622 treated mutants than untreated PMP22tg mice (Figure 6d). In contrast, no difference was seen between both groups when comparing the number of NCAM+ myelin-related profiles (Figure 6e). However, we noted a stronger immunoreactivity of NCAM+ myelin profiles in untreated PMP22tg mice compared with PLX5622 treated PMP22tg mice.

To further determine changes in the differentiation phenotype of Schwann cells during development and in adulthood, the relative mRNA expression of distinct marker genes (Fledrich et al., 2014; Fledrich, Kungl, et al., 2019; Jessen et al., 2015) was analyzed in femoral quadriceps nerves by qPCR. At 21 days and 6 months of age, PMP22tg mutants displayed an increased expression of several markers of immature and dedifferentiated Schwann cells compared to WT mice (Figure 7). Interestingly, at younger ages (21 days of age), the genuine dedifferentiation markers *Nrg1/I* and *Shh* showed a higher increase in expression in treated PMP22tg mutants compared to the untreated mutants (Figure 7a). At 6 months of age, none of the investigated markers was influenced by PLX5622 treatment in PMP22tg mice (Figure 7b). These observations reflect an early impact of macrophages on the abnormal differentiation state of Schwann cells in a mouse model of CMT1A.

3.4 | Early postnatal PLX5622 treatment does not alleviate the demyelinating phenotype in a mouse model for CMT1X

In our previous approach, the pharmacological depletion of macrophages from 3 months of age resulted in a persistent mitigation of axonal damage and an improved clinical phenotype in a mouse model for CMT1X (Klein et al., 2015). In contrast, features indicative of demyelination were not ameliorated in peripheral nerves of these mice after 3 or 9 months of macrophage targeting (Klein et al., 2015). Since we here show that early PLX5622 treatment in PMP22tg mutants resulted in a reduction of demyelinating features, we tested the hypothesis that early treatment in Cx32def mice might also alleviate their demyelinating phenotype, assuming a similar impact of early macrophage targeting in distinct CMT1 models. Comparable to our observations in PMP22tg mice (see Figure 3), treating Cx32def mice with PLX5622 resulted in a ~70% reduction in the numbers of endoneurial macrophages at 4 months of age (Figure S5a). Interestingly, features indicative of demyelination were not reduced in Cx32def mice compared to untreated controls (Figure S5b–e). These data reveal a fundamental difference between Cx32def mice and PMP22tg mice regarding the early impact of macrophages on demyelinating pathomechanisms.

4 | DISCUSSION

Previous studies from our laboratory demonstrated the pathogenic impact of macrophage-related inflammation in peripheral nerves of two distinct models of CMT1 neuropathies. Here we show that pharmacological targeting of macrophage-mediated nerve inflammation is a feasible approach to mitigate the neuropathy in a third mouse model, representing the most common type - CMT1A. Rescuing pathological demyelinating features by early PLX5622 treatment (this study) or by reduced CCL2-expression (Kohl et al., 2010), clearly demonstrates that macrophage involvement is not a general epiphenomenon in diseased nerves of CMT1A mice, but promotes demyelination. By contrast, we unequivocally identified hypermyelination - as opposed to demyelination - as a typical, disease-specific feature being independent of macrophage activation (Kohl et al., 2010 and this study). Importantly, one of the major take-home messages of our study is that attenuation of demyelination in PMP22tg mice by macrophage targeting requires an early, postnatal time window to achieve treatment success. This seems to be specific for PMP22tg mice, as a similar treatment approach failed to alleviate myelinopathy in Cx32def mice. Importantly, if this time window has passed, as demonstrated in mice treated from 3 months onwards (Klein et al., 2015), CSF-1Ri treatment still leads to a robust reduction of macrophage numbers, but demyelination and disease progression continue. Of note, recent unpublished data from our laboratory showed that starting the treatment in PMP22tg mice at 4 weeks also fails to ameliorate the demyelinating phenotype (data not shown), suggesting a rather narrow time window for successful treatment. The success in robustly alleviating the neuropathy by genetically mediated CCL2- (Kohl et al., 2010) or CSF-1-deficiency (CSF-1op, this study) from the onset, is in line with the need for an early macrophage modulation in CMT1A models. Based on these combined observations, the question emerges about the mechanisms of disease progression when macrophages are targeted after this putative critical time window of treatment. It is conceivable that the remaining macrophages, possibly independent of CSF-1R (Chitu et al., 2020; Elmore et al., 2018), are still sufficient to mediate demyelination. The presence of foamy macrophages identified by electron microscopy and the amoeboid appearance of some remaining macrophages (unpublished observations) may suggest an activated phenotype and the possibility of an at least partial compensation for the successfully depleted cells. Future studies on phagocytic capacities of isolated nerve macrophages combined with transcriptome analysis of early treated, late treated, and untreated CMT1A mutants may be helpful to get more insights into the effect of macrophage targeting at different time points in CMT1A models.

An alternative or supplementary explanation implicates Schwann cell-mediated myelin removal as it occurs after nerve injury or in a segmental demyelination model (Belgrad et al., 2020; Brosius Lutz et al., 2017; Gomez-Sanchez et al., 2015;Jang et al., 2017; Park et al., 2019). Jang et al. propose a myelin-digesting pathway, starting with dedifferentiation-associated demyelination by Schwann cells, continued by macrophage-associated digestion (Jang et al., 2017). In an attempt to identify important molecular players initiating myelin breakdown by Schwann cells, Ying et al. (Ying et al., 2018) demonstrated the

cell membrane directed, necroptosis-related pseudokinase MLKL as driver of Schwann cell-mediated myelin destruction and clearance after injury. Importantly, Brosius Lutz et al. (2017) demonstrate the implication of Schwann cell-related Tyro3, Axl, Mer receptors as an additional mechanism of autophagy-related myelin clearance. Interestingly, promoting Schwann cell autophagy with rapamycin led to a reduction of CD11b + macrophages upon constriction injury (Marinelli et al., 2014) possibly reflecting a fine-tuned coordination between Schwann cell- and macrophage-related myelin clearance in injured peripheral nerves. Paradoxically, it was shown that myelin digestion is attenuated in Schwann cells when macrophages are depleted by clodronate (Jang et al., 2017; Park et al., 2019). While the interplay between Schwann cell-mediated myelin digestion and macrophage-mediated myelin removal contribute to myelin clearance in lesioned nerves, we failed to recognize morphological correlates of an increased, compensatory myelin removal by Schwann cells in the case of late-onset PLX5622 treatment which depletes most macrophages. This observation, however, might be related to the slow, continuously progressing myelin wasting in the CMT1A model, being far less obvious than the degenerative processes within the Schwann cells after acute injury, like autophagy and ovoid formation. Thus, it will be worthwhile to investigate Schwann cell-related mechanisms of myelin clearance in normal and late-onset macrophage-depleted CMT1A models in future studies. We anticipate clear differences to Wallerian degeneration where macrophages need to remove large amounts of emerging debris within a short time period.

Interestingly, another experimental treatment approach for CMT1A models is also dependent on an early time window: the typical differentiation defect in Schwann cells of CMT1A rats could only be reverted by soluble neuregulin-1 when the models were treated between postnatal day 6 and 18 (Fledrich et al., 2014). Similar to our observations, a genetic and thus early upregulation of neuregulin-1 expression ameliorates disease in the same CMT1A mouse model that we used (Fledrich et al., 2014). Although endogenous neuregulin-1 is normally not expressed by Schwann cells throughout development, acute and chronic nerve injury leads to a de novo expression of the soluble type I isoform of neuregulin-1, rendering it a genuine dedifferentiation marker. This glial Nrg1/I expression supports nerve repair when transiently expressed after acute nerve injury (Stassart et al., 2013), but turns into a detrimental overstimulation of Schwann cells on the long term when persistently expressed as in models of chronic CMT1A (Fledrich, et al., 2019). Importantly, however, like in acute nerve injury in adult individuals, early postnatal Nrg1/I induction in Schwann cells constitutes a pro-myelinating signal in CMT1A models (Fledrich, et al., 2019). Further increased glial *Nrg1/I* expression in PMP22tg mice after PLX5622 treatment (along with *Shh*, another specific repair marker, Jessen & Mirsky, 2019) may therefore reflect and contribute to improved postnatal myelination in PMP22tg mice. These combined observations raised the question of the interrelationship of macrophage activity and neuregulin-1 expression. In the context of macrophages as potent drivers of Schwann cell dedifferentiation, our data suggest a molecular facet of nerve repair that might be suppressed by macrophages. Moreover, the recently described immunomodulatory role of neuregulin-1 in promoting a beneficial phenotype of macrophages is an interesting finding (Kataria et al., 2019; Kataria et al., 2021) of putative relevance for CMT1A models. Based on these complex considerations on the molecular role of macrophage-related functions in the diseased nerves of PMP22tg mice, a challenging future approach would be to repeat our experiments in CMT1A rats (Sereda et al., 1996).

While neuregulin-1 exposure caused a correction of the typical differentiation defect of myelinating Schwann cells in rodent models of CMT1A (Fledrich et al., 2014), we hypothesized that early therapeutic depletion of macrophages may cause similar changes. Among several molecules investigated, NCAM expression in early treated and untreated PMP22tg mice was particularly interesting. Under normal conditions, this molecule is strongly expressed in peripheral nerves before myelination but becomes scarcely detectable when Schwann cells start to form compact myelin (Martini & Schachner, 1986). In contrast, NCAM is amply expressed in myelinating Schwann cells of dysmyelinating mutants like in mice homozygously deficient for MPZ (P0; Giese et al., 1992) or in PMP22tg mice (Klein et al., 2014 and this study) where Schmidt-Lanterman-Incisures are strongly immunoreactive. Moreover, supernumerary Schwann cells in various CMT1 models are NCAM-positive (Guenard et al., 1996; Hanemann et al., 1997; Klein et al., 2014), confirming NCAM as a marker of abnormal Schwann cell differentiation. As in previous studies we focused on immunohistochemical stainings rather than on Western blot or qPCR analysis, aiming to analyze NCAM expression on a cellular level. Interestingly, in unpublished experiments where we also found increased protein levels by immunofluorescence, we failed to show an upregulation of *Ncam1* at the mRNA level when comparing peripheral nerves from PMP22tg and WT mice. While this was initially unexpected, it is important to note that most isoforms of NCAM are transmembrane proteins linked to the spectrin cytoskeleton (Sytnyk et al., 2017). This might explain some of the differences regarding transcript and protein levels in the nerve. Corroborating our previous findings (Klein et al., 2014), NCAM-positive Schwann cells were abundant in 6-month-old PMP22tg mice, but they were significantly reduced in numbers when macrophages were targeted. The reduced numbers of NCAM-positive profiles around nerve fibers can be correlated with fewer onion bulbs surrounding thinly myelinated or demyelinated axons, thus implicating abnormally differentiated Schwann cells. This might be a consequence of alleviated nerve damage. Particularly interesting was the attenuated NCAM-immunoreactivity of mutant myelinating Schwann cells upon macrophage targeting, possibly reflecting a direct impact of macrophages on the disease-promoting, abnormal Schwann cell differentiation in CMT1A models. Interestingly, from other pathological conditions, like cancer, it is known that tumor-associated macrophages (TAM) play a crucial role in the dedifferentiation process of tumor cells (for review see Muller et al., 2020).

At present, treating CMT1 disorders is still limited to symptomatic approaches and rehabilitation, although promising attempts have been previously performed in the respective animal models (Fledrich et al., 2012; Jerath & Shy, 2015; Klein & Martini, 2016; Prukop et al., 2019; Prukop et al., 2020). Recently, a couple of studies focusing on gene therapeutic approaches used distinct vectors to correct

dysfunctional gene expression or to silence overexpressed genes in the respective animal models (Gautier et al., 2021; Kagiava et al., 2016; Kagiava et al., 2019; Kagiava et al., 2021; Pisciotta et al., 2021; Sargiannidou et al., 2020; Zhao et al., 2018). As long as such causative therapies are not established, we consider macrophage targeting as an alternative approach to mitigate disease outcome (Klein et al., 2015; Klein & Martini, 2016). However, the simultaneous, inevitable depletion of microglial cells upon CSF-1R inhibition has to be critically considered (Berve et al., 2020; Elmore et al., 2014; Elmore et al., 2018; Groh et al., 2019; Lei et al., 2020; Priller & Prinz, 2019; Spangenberg et al., 2019), particularly due to the multiple immunological and neurobiological functions of these cells (Prinz et al., 2021). Another caveat is the need for an early onset of treatment in CMT1A models that certainly makes the translation to clinics problematic. Thus, development of novel tools targeting neuroinflammation specifically in the PNS is needed. Based on these current limitations of pharmacological targeting of macrophages with PLX5622, it is interesting to note that we recently identified moderate physical exercise as a safe approach to mitigate nerve pathology and clinical outcome in a model of CMT1X. This was likely mediated by modulating macrophage activation and upregulating trophic factors that preserved myelin integrity (Klein et al., 2021). Since physical exercise additionally supports and improves health and well-being in general (Mori et al., 2020; Pedersen, 2017; Sman et al., 2015), applying this to CMT1A and other subtypes of CMT might be a promising approach to alleviate the neuropathy. It would be interesting to investigate whether this and possibly other approaches in treating CMT1A are also dependent on early onset, as we here show for pharmacological macrophage depletion with PLX5622. If so, our present study may be of substantial help to understand therapeutic failures in CMT1A when the respective treatment approaches started in adult individuals.

ACKNOWLEDGMENTS

The authors are grateful to Heinrich Blazyca, Silke Loserth, and Bettina Meyer for expert technical assistance and to Anja Weidner and Thomas Bimmerlein for attentive animal care. The authors thank Plexxikon Inc. for constant, generous support, providing PLX5622 chow and performing mass spectrometry to determine PLX5622 concentrations in plasma of treated mutants. The study was supported by the Federal Ministry of Education and Research (CMT-NET; Projects R4 [Rudolf Martini] and R5 [Ruth Stassart]) and the Elite Network of Bavaria "Translational Neuroscience".

CONFLICT OF INTEREST

The authors declare no conflicts of interest.

AUTHOR CONTRIBUTION

Dennis Klein, Janos Groh, and Rudolf Martini designed research. Dennis Klein, Janos Groh, Xidi Yuan, and Robert Fledrich performed research. Dennis Klein, Janos Groh, Xidi Yuan, Kristina Berve, Ruth Stassart, Robert Fledrich, and Rudolf Martini analyzed data. Dennis Klein and Rudolf Martini wrote the manuscript with input from all authors. All authors discussed the results and commented on the final manuscript.

DATA AVAILABILITY STATEMENT

The data that support the findings of this study are available from the corresponding author upon reasonable request.

ORCID

Dennis Klein https://orcid.org/0000-0002-0476-445X
Janos Groh https://orcid.org/0000-0002-7628-0163
Xidi Yuan https://orcid.org/0000-0001-7392-2514
Ruth Stassart https://orcid.org/0000-0002-5919-1652
Robert Fledrich https://orcid.org/0000-0001-5323-7958
Rudolf Martini https://orcid.org/0000-0002-5463-5592

REFERENCES

Amann, L., & Prinz, M. (2020). The origin, fate and function of macrophages in the peripheral nervous system - an update. *International Immunology*, *32*, 709–717. https://doi.org/10.1093/intimm/dxaa030

Anzini, P., Neuberg, D. H., Schachner, M., Nelles, E., Willecke, K., Zielasek, J., Toyka, K. V., Suter, U., & Martini, R. (1997). Structural abnormalities and deficient maintenance of peripheral nerve myelin in mice lacking the gap junction protein connexin 32. *The Journal of Neuroscience: The Official Journal of the Society for Neuroscience*, *17*(12), 4545–4551.

Belgrad, J., De Pace, R., & Fields, R. D. (2020). Autophagy in myelinating glia. *The Journal of Neuroscience*, *40*(2), 256–266. https://doi.org/10.1523/JNEUROSCI.1066-19.2019

Berve, K., West, B. L., Martini, R., & Groh, J. (2020). Sex- and region-biased depletion of microglia/macrophages attenuates CLN1 disease in mice. *Journal of Neuroinflammation*, *17*(1), 323. https://doi.org/10.1186/s12974-020-01996-x

Bethea, J. R., & Fischer, R. (2021). Role of peripheral immune cells for development and recovery of chronic pain. *Frontiers in Immunology*, *12*, 641588. https://doi.org/10.3389/fimmu.2021.641588

Brosius Lutz, A., Chung, W. S., Sloan, S. A., Carson, G. A., Zhou, L., Lovelett, E., Posada, S., Zuchero, J. B., & Barres, B. A. (2017). Schwann cells use TAM receptor-mediated phagocytosis in addition to autophagy to clear myelin in a mouse model of nerve injury. *Proceedings of the National Academy of Sciences of the United States of America*, *114*(38), 8072–8080. https://doi.org/10.1073/pnas.1710566114

Carenini, S., Maurer, M., Werner, A., Blazyca, H., Toyka, K. V., Schmid, C. D., Raivich, G., & Martini, R. (2001). The role of macrophages in demyelinating peripheral nervous system of mice heterozygously deficient in p0. *The Journal of Cell Biology*, *152*(2), 301–308.

Cattin, A. L., Burden, J. J., Van Emmenis, L., Mackenzie, F. E., Hoving, J. J., Garcia Calavia, N., Guo, Y., McLaughlin, M., Rosenberg, L. H., Quereda, V., Jamecna, D., Napoli, I., Parrinello, S., Enver, T., Ruhrberg, C., & Lloyd, A. C. (2015). Macrophage-Induced Blood Vessels Guide Schwann Cell-Mediated Regeneration of Peripheral Nerves. *Cell*, *162*(5), 1127–1139. https://doi.org/10.1016/j.cell.2015.07.021

Chitu, V., Biundo, F., Shlager, G. G. L., Park, E. S., Wang, P., Gulinello, M. E., Gokhan, S., Ketchum, H. C., Saha, K., DeTure, M. A., Dickson, D. W., Wszolek, Z. K., Zheng, D., Croxford, A. L., Becher, B., Sun, D., Mehler, M. F., & Stanley, E. R. (2020). Microglial Homeostasis Requires Balanced CSF-1/CSF-2 Receptor Signaling. *Cell Reports*, *30*(9), 3004–3019. e5. https://doi.org/10.1016/j.celrep.2020.02.028

Elmore, M. R., Najafi, A. R., Koike, M. A., Dagher, N. N., Spangenberg, E. E., Rice, R. A., Kitazawa, M., Matusow, B., Nguyen, H., West, B. L., & Green, K. N. (2014). Colony-stimulating factor 1 receptor signaling is necessary for microglia viability, unmasking a microglia progenitor cell in the adult brain. *Neuron*, *82*(2), 380–397. https://doi.org/10.1016/j.neuron.2014.02.040

Elmore, M. R. P., Hohsfield, L. A., Kramar, E. A., Soreq, L., Lee, R. J., Pham, S. T., Najafi, A. R., Spangenberg, E. E., Wood, M. A., West, B. L.,

& Green, K. N. (2018). Replacement of microglia in the aged brain reverses cognitive, synaptic, and neuronal deficits in mice. *Aging Cell*, *17*(6), e12832. https://doi.org/10.1111/acel.12832

Faul, F., Erdfelder, E., Lang, A. G., & Buchner, A. (2007). G*power 3: A flexible statistical power analysis program for the social, behavioral, and biomedical sciences. *Behavior Research Methods*, *39*(2), 175–191. https://doi.org/10.3758/Bf03193146

Fischer, S., Weishaupt, A., Troppmair, J., & Martini, R. (2008). Increase of MCP-1 (CCL2) in myelin mutant Schwann cells is mediated by MEK-ERK signaling pathway. *Glia*, *56*(8), 836–843.

Fledrich, R., Akkermann, D., Schutza, V., Abdelaal, T. A., Hermes, D., Schaffner, E., Soto-Bernardini, M. C., Gotze, T., Klink, A., Kusch, K., Krueger, M., Kungl, T., Frydrychowicz, C., Mobius, W., Bruck, W., Mueller, W. C., Bechmann, I., Sereda, M. W., Schwab, M. H., Nave, K. A., & Stassart, R. M. (2019). NRG1 type I dependent autoparacrine stimulation of Schwann cells in onion bulbs of peripheral neuropathies. *Nature Communications*, *10*(1), 1467. https://doi.org/10.1038/s41467-019-09385-6

Fledrich, R., Kungl, T., Nave, K. A., & Stassart, R. M. (2019). Axo-glial interdependence in peripheral nerve development. *Development*, *146* (21), dev151704. https://doi.org/10.1242/dev.151704

Fledrich, R., Stassart, R. M., Klink, A., Rasch, L. M., Prukop, T., Haag, L., Czesnik, D., Kungl, T., Abdelaal, T. A., Keric, N., Stadelmann, C., Bruck, W., Nave, K. A., & Sereda, M. W. (2014). Soluble neuregulin-1 modulates disease pathogenesis in rodent models of Charcot-Marie-tooth disease 1A. *Nature Medicine*, *20*(9), 1055–1061. https://doi.org/10.1038/nm.3664

Fledrich, R., Stassart, R. M., & Sereda, M. W. (2012). Murine therapeutic models for Charcot-Marie-tooth (CMT) disease. *British Medical Bulletin*, *102*, 89–113. https://doi.org/10.1093/bmb/lds010

Frei, R., Mötzing, S., Kinkelin, I., Schachner, M., Koltzenburg, M., & Martini, R. (1999). Loss of distal axons and sensory Merkel cells and features indicative of muscle denervation in hindlimbs of P0-deficient mice. *The Journal of Neuroscience*, *19*, 6058–6067.

Gautier, B., Hajjar, H., Soares, S., Berthelot, J., Deck, M., Abbou, S., Campbell, G., Ceprian, M., Gonzalez, S., Fovet, C. M., Schutza, V., Jouvenel, A., Rivat, C., Zerah, M., Francois, V., Le Guiner, C., Aubourg, P., Fledrich, R., & Tricaud, N. (2021). AAV2/9-mediated silencing of PMP22 prevents the development of pathological features in a rat model of Charcot-Marie-tooth disease 1 a. *Nature Communications*, *12*(1), 2356. https://doi.org/10.1038/s41467-021-22593-3

Giese, K. P., Martini, R., Lemke, G., Soriano, P., & Schachner, M. (1992). Mouse P0 gene disruption leads to hypomyelination, abnormal expression of recognition molecules, and degeneration of myelin and axons. *Cell*, *71*(4), 565–576.

Gomez-Sanchez, J. A., Carty, L., Iruarrizaga-Lejarreta, M., Palomo-Irigoyen, M., Varela-Rey, M., Griffith, M., Hantke, J., Macias-Camara, N., Azkargorta, M., Aurrekoetxea, I., De Juan, V. G., Jefferies, H. B., Aspichueta, P., Elortza, F., Aransay, A. M., Martinez-Chantar, M. L., Baas, F., Mato, J. M., Mirsky, R., Woodhoo, A., … Jessen, K. R. (2015). Schwann cell autophagy, myelinophagy, initiates myelin clearance from injured nerves. *The Journal of Cell Biology*, *210*(1), 153–168. https://doi.org/10.1083/jcb.201503019

Goodfellow, J. A., & Willison, H. J. (2018). Gangliosides and autoimmune peripheral nerve diseases. *Progress in Molecular Biology and Translational Science*, *156*, 355–382. https://doi.org/10.1016/bs.pmbts.2017.12.010

Groh, J., Heinl, K., Kohl, B., Wessig, C., Greeske, J., Fischer, S., & Martini, R. (2010). Attenuation of MCP-1/CCL2 expression ameliorates neuropathy in a mouse model for Charcot-Marie-tooth 1X. *Human Molecular Genetics*, *19*(18), 3530–3543.

Groh, J., Klein, D., Berve, K., West, B. L., & Martini, R. (2019). Targeting microglia attenuates neuroinflammation-related neural damage in mice carrying human PLP1 mutations. *Glia*, *67*(2), 277–290. https://doi.org/10.1002/glia.23539

Groh, J., Klein, D., Kroner, A., & Martini, R. (2015). Inflammation in the pathogenesis of inherited peripheral neuropathies. In S. David (Ed.), *Neuroinflammation: New insights into beneficial and detrimental functions* (1st ed., pp. 123–137). John Wiley & Sons, Inc.

Groh, J., Klein, I., Hollmann, C., Wettmarshausen, J., Klein, D., & Martini, R. (2015). CSF-1-activated macrophages are target-directed and essential mediators of schwann cell dedifferentiation and dysfunction in Cx32-deficient mice. *Glia*, *63*(6), 977–986. https://doi.org/10.1002/glia.22796

Groh, J., Weis, J., Zieger, H., Stanley, E. R., Heuer, H., & Martini, R. (2012). Colony-stimulating factor-1 mediates macrophage-related neural damage in a model for Charcot-Marie-tooth disease type 1X. *Brain: A Journal of Neurology*, *135*(1), 88–104. https://doi.org/10.1093/brain/awr283

Guenard, V., Montag, D., Schachner, M., & Martini, R. (1996). Onion bulb cells in mice deficient for myelin genes share molecular properties with immature, differentiated non-myelinating, and denervated Schwann cells. *Glia*, *18*(1), 27–38. https://doi.org/10.1002/(SICI)1098-1136(199609)18:1<27::AID-GLIA3>3.0.CO;2-0

Hanemann, C. O., Gabreels-Festen, A. A., Stoll, G., & Muller, H. W. (1997). Schwann cell differentiation in Charcot-Marie-tooth disease type 1A (CMT1A): Normal number of myelinating Schwann cells in young CMT1A patients and neural cell adhesion molecule expression in onion bulbs. *Acta Neuropathologica*, *94*(4), 310–315.

Ho, T. W., McKhann, G. M., & Griffin, J. W. (1998). Human autoimmune neuropathies. *Annual Reviews in the Neurosciences*, *21*, 187–226.

Huxley, C., Passage, E., Robertson, A. M., Youl, B., Huston, S., Manson, A., Saberan-Djoniedi, D., Figarella-Branger, D., Pellissier, J. F., Thomas, P. K., & Fontes, M. (1998). Correlation between varying levels of PMP22 expression and the degree of demyelination and reduction in nerve conduction velocity in transgenic mice. *Human Molecular Genetics*, *7*(3), 449–458. https://doi.org/10.1093/hmg/7.3.449

Jang, S. Y., Yoon, B. A., Shin, Y. K., Yun, S. H., Jo, Y. R., Choi, Y. Y., Ahn, M., Shin, T., Park, J. I., Kim, J. K., & Park, H. T. (2017). Schwann cell dedifferentiation-associated demyelination leads to exocytotic myelin clearance in inflammatory segmental demyelination. *Glia*, *65*(11), 1848–1862. https://doi.org/10.1002/glia.23200

Jerath, N. U., & Shy, M. E. (2015). Hereditary motor and sensory neuropathies: Understanding molecular pathogenesis could lead to future treatment strategies. *Biochimica et Biophysica Acta*, *1852*(4), 667–678. https://doi.org/10.1016/j.bbadis.2014.07.031

Jessen, K. R., & Mirsky, R. (2019). The success and failure of the Schwann cell response to nerve injury. *Frontiers in Cellular Neuroscience*, *13*, 33. https://doi.org/10.3389/fncel.2019.00033

Jessen, K. R., Mirsky, R., & Lloyd, A. C. (2015). Schwann cells: Development and role in nerve repair. *Cold Spring Harbor Perspectives in Biology*, *7*(7), a020487. https://doi.org/10.1101/cshperspect.a020487

Kagiava, A., Karaiskos, C., Richter, J., Tryfonos, C., Jennings, M. J., Heslegrave, A. J., Sargiannidou, I., Stavrou, M., Zetterberg, H., Reilly, M. M., Christodoulou, C., Horvath, R., & Kleopa, K. A. (2021). AAV9-mediated Schwann cell-targeted gene therapy rescues a model of demyelinating neuropathy. *Gene therapy.*, *28*, 659–675. https://doi.org/10.1038/s41434-021-00250-0

Kagiava, A., Richter, J., Tryfonos, C., Karaiskos, C., Heslegrave, A. J., Sargiannidou, I., Rossor, A. M., Zetterberg, H., Reilly, M. M., Christodoulou, C., & Kleopa, K. A. (2019). Gene replacement therapy after neuropathy onset provides therapeutic benefit in a model of CMT1X. *Human Molecular Genetics*, *28*, 3528–3542. https://doi.org/10.1093/hmg/ddz199

Kagiava, A., Sargiannidou, I., Theophilidis, G., Karaiskos, C., Richter, J., Bashiardes, S., Schiza, N., Nearchou, M., Christodoulou, C., Scherer, S. S., & Kleopa, K. A. (2016). Intrathecal gene therapy rescues a model of demyelinating peripheral neuropathy. *Proceedings of the National Academy of Sciences of the United States of America*, *113*(17), 2421–2429. https://doi.org/10.1073/pnas.1522202113

Kataria, H., Alizadeh, A., & Karimi-Abdolrezaee, S. (2019). Neuregulin-1/ErbB network: An emerging modulator of nervous system injury and repair. *Progress in Neurobiology*, *180*, 101643. https://doi.org/10.1016/j.pneurobio.2019.101643

Kataria, H., Hart, C. G., Alizadeh, A., Cossoy, M., Kaushik, D. K., Bernstein, C. N., Marrie, R. A., Yong, V. W., & Karimi-Abdolrezaee, S. (2021). Neuregulin-1 beta 1 is implicated in pathogenesis of multiple sclerosis. *Brain*, *144*(1), 162–185. https://doi.org/10.1093/brain/awaa385

Klein, D., Groh, J., Wettmarshausen, J., & Martini, R. (2014). Nonuniform molecular features of myelinating Schwann cells in models for CMT1: Distinct disease patterns are associated with NCAM and c-Jun upregulation. *Glia*, *62*(5), 736–750. https://doi.org/10.1002/glia.22638

Klein, D., & Martini, R. (2016). Myelin and macrophages in the PNS: An intimate relationship in trauma and disease. *Brain Research*, *1641*(Pt A), 130–138. https://doi.org/10.1002/glia.22638

Klein, D., Patzko, A., Schreiber, D., van Hauwermeiren, A., Baier, M., Groh, J., West, B. L., & Martini, R. (2015). Targeting the colony stimulating factor 1 receptor alleviates two forms of Charcot-Marie-tooth disease in mice. *Brain: A Journal of Neurology*, *138*(11), 3193–3205. https://doi.org/10.1093/brain/awv240

Klein, D., Yuan, X., Weiss, E. M., & Martini, R. (2021). Physical exercise mitigates neuropathic changes in an animal model for Charcot-Marie-tooth disease 1X. *Experimental Neurology*, *343*, 113786. https://doi.org/10.1016/j.expneurol.2021.113786

Kobsar, I., Berghoff, M., Samsam, M., Wessig, C., Maurer, M., Toyka, K. V., & Martini, R. (2003). Preserved myelin integrity and reduced axonopathy in connexin32-deficient mice lacking the recombination activating gene-1. *Brain*, *126*(Pt 4), 804–813.

Kobsar, I., Hasenpusch-Theil, K., Wessig, C., Muller, H. W., & Martini, R. (2005). Evidence for macrophage-mediated myelin disruption in an animal model for Charcot-Marie-tooth neuropathy type 1A. *Journal of Neuroscience Research*, *81*(6), 857–864.

Kohl, B., Fischer, S., Groh, J., Wessig, C., & Martini, R. (2010). MCP-1/CCL2 modifies axon properties in a PMP22-overexpressing mouse model for Charcot-Marie-tooth 1A neuropathy. *The American Journal of Pathology*, *176*(3), 1390–1399.

Kolter, J., Feuerstein, R., Zeis, P., Hagemeyer, N., Paterson, N., d'Errico, P., Baasch, S., Amann, L., Masuda, T., Losslein, A., Gharun, K., Meyer-Luehmann, M., Waskow, C., Franzke, C. W., Grun, D., Lammermann, T., Prinz, M., & Henneke, P. (2019). A subset of skin macrophages contributes to the surveillance and regeneration of local nerves. *Immunity*, *50*(6), 1482–1497. e7. https://doi.org/10.1016/j.immuni.2019.05.009

Kolter, J., Kierdorf, K., & Henneke, P. (2020). Origin and differentiation of nerve-associated macrophages. *Journal of Immunology*, *204*(2), 271–279. https://doi.org/10.4049/jimmunol.1901077

Lei, F., Cui, N., Zhou, C., Chodosh, J., Vavvas, D. G., & Paschalis, E. I. (2020). CSF1R inhibition by a small-molecule inhibitor is not microglia specific; affecting hematopoiesis and the function of macrophages. *Proceedings of the National Academy of Sciences of the United States of America*, *117*(38), 23336–23338. https://doi.org/10.1073/pnas.1922788117

Marinelli, S., Nazio, F., Tinari, A., Ciarlo, L., D'Amelio, M., Pieroni, L., … Pavone, F. (2014). Schwann cell autophagy counteracts the onset and chronification of neuropathic pain. *Pain*, *155*(1), 93–107. https://doi.org/10.1016/j.pain.2013.09.013

Martini, R., Klein, D., & Groh, J. (2013). Similarities between inherited demyelinating neuropathies and Wallerian degeneration: An old repair program may cause myelin and axon perturbation under nonlesion conditions. *The American Journal of Pathology*, *183*(3), 655–660. https://doi.org/10.1016/j.ajpath.2013.06.002

Martini, R., & Schachner, M. (1986). Immunoelectron microscopic localization of neural cell adhesion molecules (L1, N-CAM, and MAG) and their shared carbohydrate epitope and myelin basic protein in developing sciatic nerve. *The Journal of Cell Biology*, *103*(6 Pt 1), 2439–2448.

Martini, R., & Willison, H. (2016). Neuroinflammation in the peripheral nerve: Cause, modulator, or bystander in peripheral neuropathies? *Glia*, *64*(4), 475–486. https://doi.org/10.1002/glia.22899

Mori, L., Signori, A., Prada, V., Pareyson, D., Piscosquito, G., Padua, L., Pazzaglia, C., Fabrizi, G. M., Picelli, A., Schenone, A., & TreSPE study group (2020). Treadmill training in patients affected by Charcot-Marie-tooth neuropathy: Results of a multicenter, prospective, randomized, single-blind, controlled study. *European journal of neurology: the official journal of the European Federation of Neurological Societies*, *27*(2), 280–287. https://doi.org/10.1111/ene.14074

Muller, L., Tunger, A., Plesca, I., Wehner, R., Temme, A., Westphal, D., Meier, F., Bachmann, M., & Schmitz, M. (2020). Bidirectional crosstalk between cancer stem cells and immune cell subsets. *Frontiers in Immunology*, *11*, 140. https://doi.org/10.3389/fimmu.2020.00140

Nelles, E., Butzler, C., Jung, D., Temme, A., Gabriel, H. D., Dahl, U., Traub, O., Stumpel, F., Jungermann, K., Zielasek, J., Toyka, K. V., Dermietzel, R., … Willecke, K. (1996). Defective propagation of signals generated by sympathetic nerve stimulation in the liver of connexin32-deficient mice. *Proceedings of the National Academy of Sciences of the United States of America*, *93*(18), 9565–9570. https://doi.org/10.1073/pnas.93.18.9565

Park, H. T., Kim, J. K., & Tricaud, N. (2019). The conceptual introduction of the "demyelinating Schwann cell" in peripheral demyelinating neuropathies. *Glia*, *67*(4), 571–581. https://doi.org/10.1002/glia.23509

Pedersen, B. K. (2017). Anti-inflammatory effects of exercise: Role in diabetes and cardiovascular disease. *European Journal of Clinical Investigation*, *47*(8), 600–611. https://doi.org/10.1111/eci.12781

Pisciotta, C., Saveri, P., & Pareyson, D. (2021). Updated review of therapeutic strategies for Charcot-Marie-tooth disease and related neuropathies. *Expert Review of Neurotherapeutics*, *21*(6), 701–713. https://doi.org/10.1080/14737175.2021.1935242

Priller, J., & Prinz, M. (2019). Targeting microglia in brain disorders. *Science*, *365*(6448), 32–33. https://doi.org/10.1126/science.aau9100

Prinz, M., Masuda, T., Wheeler, M. A., & Quintana, F. J. (2021). Microglia and central nervous system-associated macrophages-from origin to disease modulation. *Annual Review of Immunology*, *39*, 251–277. https://doi.org/10.1146/annurev-immunol-093019-110159

Prukop, T., Stenzel, J., Wernick, S., Kungl, T., Mroczek, M., Adam, J., Ewers, D., Nabirotchkin, S., Nave, K. A., Hajj, R., Cohen, D., & Sereda, M. W. (2019). Early short-term PXT3003 combinational therapy delays disease onset in a transgenic rat model of Charcot-Marie-tooth disease 1A (CMT1A). *PLoS One*, *14*(1), e0209752. https://doi.org/10.1371/journal.pone.0209752

Prukop, T., Wernick, S., Boussicault, L., Ewers, D., Jager, K., Adam, J., Winter, L., Quintes, S., Linhoff, L., Barrantes-Freer, A., Bartl, M., Czesnik, D., Zschuntzsch, J., Schmidt, J., Primas, G., Laffaire, J., Rinaudo, P., Brureau, A., Nabirotchkin, S., Schwab, M. H., … Sereda, M. W. (2020). Synergistic PXT3003 therapy uncouples neuromuscular function from dysmyelination in male Charcot-Marie-tooth disease type 1A (CMT1A) rats. *Journal of Neuroscience Research*, *98*(10), 1933–1952. https://doi.org/10.1002/jnr.24679

Sargiannidou, I., Kagiava, A., & Kleopa, K. A. (2020). Gene therapy approaches targeting Schwann cells for demyelinating neuropathies. *Brain Research*, *1728*, 146572. https://doi.org/10.1016/j.brainres.2019.146572

Sereda, M., Griffiths, I., Puhlhofer, A., Stewart, H., Rossner, M. J., Zimmerman, F., Magyar, J. P., Schneider, A., Hund, E., Meinck, H. M., Suter, U., & Nave, K. A. (1996). A transgenic rat model of Charcot-Marie-tooth disease. *Neuron*, *16*(5), 1049–1060.

Shepherd, A. J., Mickle, A. D., Golden, J. P., Mack, M. R., Halabi, C. M., de Kloet, A. D., Samineni, V. K., Kim, B. S., Krause, E. G., Gereau, R. W. t., & Mohapatra, D. P. (2018). Macrophage angiotensin II type 2 receptor triggers neuropathic pain. *Proceedings of the National Academy of Sciences of the United States of America*, *115*(34), 8057–8066. https://doi.org/10.1073/pnas.1721815115

Sman, A. D., Hackett, D., Fiatarone Singh, M., Fornusek, C., Menezes, M. P., & Burns, J. (2015). Systematic review of exercise for Charcot-Marie-tooth disease. *Journal of the Peripheral Nervous System*, *20*(4), 347–362. https://doi.org/10.1111/jns.12116

Sommer, C., Leinders, M., & Uceyler, N. (2018). Inflammation in the pathophysiology of neuropathic pain. *Pain*, *159*(3), 595–602. https://doi.org/10.1097/j.pain.0000000000001122

Spangenberg, E., Severson, P. L., Hohsfield, L. A., Crapser, J., Zhang, J., Burton, E. A., Zhang, Y., Spevak, W., Lin, J., Phan, N. Y., Habets, G., Rymar, A., Tsang, G., Walters, J., Nespi, M., Singh, P., Broome, S., Ibrahim, P., Zhang, C., Bollag, G., & Green, K. N. (2019). Sustained microglial depletion with CSF1R inhibitor impairs parenchymal plaque development in an Alzheimer's disease model. *Nature Communications*, *10*(1), 3758. https://doi.org/10.1038/s41467-019-11674-z

Stassart, R. M., Fledrich, R., Velanac, V., Brinkmann, B. G., Schwab, M. H., Meijer, D., Sereda, M. W., & Nave, K. A. (2013). A role for Schwann cell-derived neuregulin-1 in remyelination. *Nature Neuroscience*, *16*(1), 48–54. https://doi.org/10.1038/nn.3281

Stratton, J. A., Holmes, A., Rosin, N. L., Sinha, S., Vohra, M., Burma, N. E., Trang, T., Midha, R., & Biernaskie, J. (2018). Macrophages regulate Schwann cell maturation after nerve injury. *Cell Reports*, *24*(10), 2561–2572.e6. https://doi.org/10.1016/j.celrep.2018.08.004

Sytnyk, V., Leshchyns'ka, I., & Schachner, M. (2017). Neural cell adhesion molecules of the immunoglobulin superfamily regulate synapse formation, maintenance, and function. *Trends in Neurosciences*, *40*(5), 295–308. https://doi.org/10.1016/j.tins.2017.03.003

Trias, E., Kovacs, M., King, P. H., Si, Y., Kwon, Y., Varela, V., Ibarburu, S., Moura, I. C., Hermine, O., Beckman, J. S., & Barbeito, L. (2020). Schwann cells orchestrate peripheral nerve inflammation through the expression of CSF1, IL-34, and SCF in amyotrophic lateral sclerosis. *Glia*, *68*(6), 1165–1181. https://doi.org/10.1002/glia.23768

Vargas, M. E., Watanabe, J., Singh, S. J., Robinson, W. H., & Barres, B. A. (2010). Endogenous antibodies promote rapid myelin clearance and effective axon regeneration after nerve injury. *Proceedings of the National Academy of Sciences of the United States of America*, *107*(26), 11993–11998.

Wiktor-Jedrzejczak, W., Bartocci, A., Ferrante, A. W., Jr., Ahmed-Ansari, A., Sell, K. W., Pollard, J. W., & Stanley, E. R. (1990). Total absence of colony-stimulating factor 1 in the macrophage-deficient osteopetrotic (op/op) mouse. *Proceedings of the National Academy of Sciences of the United States of America*, *87*(12), 4828–4832.

Ydens, E., Amann, L., Asselbergh, B., Scott, C. L., Martens, L., Sichien, D., Mossad, O., Blank, T., De Prijck, S., Low, D., Masuda, T., Saeys, Y., Timmerman, V., Stumm, R., Ginhoux, F., Prinz, M., Janssens, S., & Guilliams, M. (2020). Profiling peripheral nerve macrophages reveals two macrophage subsets with distinct localization, transcriptome and response to injury. *Nature Neuroscience*, *23*, 676–689. https://doi.org/10.1038/s41593-020-0618-6

Ydens, E., Cauwels, A., Asselbergh, B., Goethals, S., Peeraer, L., Lornet, G., Almeida-Souza, L., Van Ginderachter, J. A., Timmerman, V., & Janssens, S. (2012). Acute injury in the peripheral nervous system triggers an alternative macrophage response. *Journal of Neuroinflammation*, *9*, 176. https://doi.org/10.1186/1742-2094-9-176

Ying, Z., Pan, C., Shao, T., Liu, L., Li, L., Guo, D., Zhang, S., Yuan, T., Cao, R., Jiang, Z., Chen, S., Wang, F., & Wang, X. (2018). Mixed lineage kinase domain-like protein MLKL breaks down myelin following nerve injury. *Molecular Cell*, *72*(3), 457–468. e5. https://doi.org/10.1016/j.molcel.2018.09.011

Yoshida, H., Hayashi, S.-I., Kunisada, T., Ogawa, M., Nishikawa, S., Okamura, H., Sudo, T., Shultz, L. D., & Nishikawa, S.-I. (1990). The murine mutation osteopetrosis is in the coding region of the macrophage colony stimulating factor gene. *Nature*, *345*, 442–444.

Yuan, X., Klein, D., Kerscher, S., West, B. L., Weis, J., Katona, I., & Martini, R. (2018). Macrophage depletion ameliorates peripheral neuropathy in aging mice. *The Journal of Neuroscience: The Official Journal of the Society for Neuroscience*, *38*(19), 4610–4620. https://doi.org/10.1523/JNEUROSCI.3030-17.2018

Zhao, H. T., Damle, S., Ikeda-Lee, K., Kuntz, S., Li, J., Mohan, A., Kim, A., Hung, G., Scheideler, M. A., Scherer, S. S., Svaren, J., Swayze, E. E., & Kordasiewicz, H. B. (2018). PMP22 antisense oligonucleotides reverse Charcot-Marie-tooth disease type 1A features in rodent models. *The Journal of Clinical Investigation*, *128*(1), 359–368. https://doi.org/10.1172/JCI96499

Zielasek, J., Martini, R., & Toyka, K. V. (1996). Functional abnormalities in P0-deficient mice resemble human hereditary neuropathies linked to P0 gene mutations. *Muscle & Nerve*, *19*(8), 946–952. https://doi.org/10.1002/(SICI)1097-4598(199608)19:8<946::AID-MUS2>3.0.CO;2-8

SUPPORTING INFORMATION

Additional supporting information may be found in the online version of the article at the publisher's website.

How to cite this article: Klein, D., Groh, J., Yuan, X., Berve, K., Stassart, R., Fledrich, R., & Martini, R. (2022). Early targeting of endoneurial macrophages alleviates the neuropathy and affects abnormal Schwann cell differentiation in a mouse model of Charcot-Marie-Tooth 1A. *Glia*, *70*(6), 1100–1116. https://doi.org/10.1002/glia.24158